FCTUC FACULDADE DE CIÊNCIAS
E TECNOLOGIA
UNIVERSIDADE DE COIMBRA

Carolina César Martins de Oliveira Alves

White Matter Perfusion Quantification with Single-Voxel Arterial Spin Labeling

Dissertação apresentada à Universidade de Coimbra para cumprimento dos requisitos necessários à obtenção do grau de Mestre em Engenharia Biomédica

Supervisors:
Dr. Rolf Pohmann
Prof. Dr. Miguel Castelo-Branco
Dr. João Pereira

Coimbra, 2015

This work was developed in collaboration with:

High Field Magnetic Resonance Group,
Max Planck Institute for Biological Cybernetics,
Tübingen, Germany

Max-Planck-Institut
für biologische Kybernetik

Esta cópia da tese é fornecida na condição de que quem a consulta reconhece que os direitos de autor são pertença do autor da tese e que nenhuma citação ou informação obtida a partir dela pode ser publicada sem a referência apropriada.

This copy of the thesis has been supplied on condition that anyone who consults it is understood to recognize that its copyright rests with its author and that no quotation from the thesis and no information derived from it may be published without proper acknowledgement.

À minha mãe.

Acknowledgements

Esta dissertação encerra em si a conclusão de mais uma etapa da minha vida e não seria de todo possível sem o acompanhamento excecional que tive, tanto a nível académico como pessoal.

Firstly in English, I would like to thank my supervisor Dr. Rolf Pohmann, for all his time, interest and support of this project. In addition, I'd like to thank the Max Planck Institute for Biological Cybernetics, for receiving me so well and giving me all the necessary tools to finish this dissertation, especially Prof. Dr. Klaus Scheffler and the High Field Magnetic Resonance group. A special thanks goes to Joana, Sahar and Paul, for all the help, fun and great coffee breaks and also to Fabian, Steffi and little Maxi, for all the friendship and kindness during my stay in Germany.

Agradeço imenso ao Dr. João Pereira todo o seu tempo e empenho nesta demanda, e pela inestimável e constante ajuda a cortar árvores com arenques.

Desejo agradecer também ao Prof. Dr. Miguel Castelo-Branco, pela sua disponibilidade em ser meu orientador e pelas oportunidades por si criadas, dirigidas aos alunos de Engenharia Biomédica, assim como ao Prof. Dr. Miguel Morgado, pelo excelente papel e acompanhamento que tem prestado ao longo dos anos como coordenador do curso de Mestrado Integrado em Engenharia Biomédica. A ambos, assim como à Dr.ª Sónia Gonçalves, agradeço também o tempo e interesse demonstrados ao constituírem o júri que avaliou a presente dissertação.

Ao Henrique agradeço todo o amor, carinho, compreensão e paciência, especialmente ao longo deste último ano. À Joaninha, à Carla, à Cátia (a minha Deutsch Schwester), aos meus Pérolas, às minhas Combatentes, aos meus giros de morrer (muito em breve todos engenheiros!), agradeço imenso por todo o companheirismo, amizade e partilha mútua de experiências nesta lindíssima cidade, que será nossa para sempre. Porque Coimbra é isto. Levo-vos comigo para a vida.

Agradeço aos meus irmãos, à minha sempre Caia e ao meu (também sempre) Rómulo. À minha mãe, por ser um exemplo de força para mim, por me ter incutido todos os valores e princípios pelos quais me rejo. Ao meu pai, que embora já tenha partido, sei que continua a olhar por mim e espero que se orgulhe do que vê.

“*The Road goes ever on and on*
Down from the door where it began.
Now far ahead the Road has gone,
And I must follow, if I can,
Pursuing it with eager feet,
Until it joins some larger way
Where many paths and errands meet.”

J. R. R. Tolkien

Abstract

Arterial Spin Labeling (ASL) is an MRI (Magnetic Resonance Imaging) technique that enables perfusion quantification in a non-invasive way, by using magnetically labeled arterial blood water as an endogenous tracer. Since it was first proposed in 1992 by Williams et al., it has seen great advancements, making it a very promising approach. However, one of its challenges when compared to other imaging modalities is the low signal-to-noise ratio when measuring in white matter (WM), mainly due to the intrinsic lower perfusion in this tissue and also its larger transit time, when compared to grey matter (GM). By combining pulsed ASL acquisition with single-voxel spectroscopic localization – a sequence termed FAIRPRESS – highly sensitive perfusion measurements in WM have been previously obtained. The first step of this project was further optimizing this sequence for quantification in healthy human subjects' WM.

Measuring activation in WM using BOLD (Blood Oxygen Level Dependent) fMRI (functional MRI), has proven to be very difficult and somewhat controversial, but even so the number of studies reporting activation in WM has seen a recent increase, mainly in the *corpus callosum* (CC) and by using interhemispheric tasks. The novel approach proposed in this project was to use perfusion fMRI, which has previously shown some advantages over BOLD in functional studies, but focusing on WM. The BOLD signal was simultaneously acquired during these experiments. The reconstruction routines and stimuli used were improved throughout the project, and field strength was also increased from the clinically used 3T to the ultra-high research field of 9.4T.

The results displayed good quantitative perfusion values using the optimized sequence in the resting brain, in both WM and GM. The activation experiments showed great promise for measuring perfusion and BOLD changes related to activation in GM. However, no significant activation in WM could be observed, which might indicate that there are no differences between the resting and activated states in WM, and that brain activation is purely restricted to GM. On the other hand, some data showed a tendency to have higher perfusion values during activation, which might imply that improved voxel positioning in the activated region of the CC could lead to significant activation measurements. Future work will combine this technique with Diffusion Tensor Imaging (DTI) tractography, in order to help in finding the best voxel position in the activated areas of the CC, for more precise measurements of WM perfusion during activation.

Resumo

Arterial Spin Labeling (ASL) é uma técnica de MRI (Magnetic Resonance Imaging) que permite a quantificação de perfusão de forma não-invasiva, usando a água do sangue arterial marcada magneticamente como um traçador endógeno. Desde o seu desenvolvimento em 1992 por Williams et al. tem vindo a ser aperfeiçoada, sendo atualmente uma técnica muito promissora. No entanto, um dos seus problemas quando comparada com outras modalidades de imagem é o baixo rácio sinal-ruído aquando medições em matéria branca, maioritariamente devido à baixa perfusão intrínseca do tecido e também ao seu maior tempo de trânsito, quando comparado com a matéria cinzenta.

Através da combinação de ASL pulsado com localização espectroscópica single-voxel – numa sequência denominada FAIRPRESS – já foram previamente obtidas medições de perfusão altamente sensíveis. O primeiro passo deste projeto foi otimizar esta sequência para quantificação de perfusão na matéria branca de voluntários saudáveis.

A medição da ativação em matéria branca usando BOLD (Blood Oxygen Level Dependent) fMRI (MRI funcional) é bastante difícil e algo controversa, mas ainda assim o número de estudos que reportam ativação neste tecido aumentou recentemente, maioritariamente no corpo caloso e usando tarefas interhemisféricas. A nova abordagem proposta neste projeto foi utilizar fMRI de perfusão, que já demonstrou algumas vantagens relativamente a BOLD em estudos funcionais, mas focando-se na matéria branca. O sinal BOLD foi simultaneamente adquirido durante estas experiências. A reconstrução e os estímulos usados foram melhorados ao longo do projeto, e a força do campo magnético utilizado foi também aumentado dos 3T usados na prática clínica para o campo ultra-elevado de 9.4T, utilizado apenas em investigação.

Os resultados demonstraram bons valores quantitativos de perfusão usando a sequência otimizada no cérebro em repouso, tanto na matéria branca como cinzenta. As experiências de ativação mostraram-se promissoras na medição de alterações na perfusão e em BOLD relacionadas com a ativação na matéria cinzenta. Contudo, não foi possível observar ativação significativa na matéria branca, o que poderá indicar que não existem diferenças entre os estados de repouso e ativação neste tecido, e que a ativação neuronal é puramente restrita à matéria cinzenta. Por outro lado, alguns dados mostraram uma tendência para terem maiores valores de perfusão aquando a ativação, o que poderá indicar que melhorando o posicionamento do voxel

na região ativa do corpo caloso, poderiam ser feitas medições de ativação significativas. No futuro, pretende-se combinar esta técnica com tractografia DTI (Diffusion Tensor Imaging), para auxiliar ao posicionamento do voxel nas áreas ativas do corpo caloso, para medições mais precisas de perfusão em matéria branca durante a ativação.

Contents

Acknowledgements vi

Abstract viii

Resumo ix

Contents xi

List of Abbreviations xiv

List of Figures xv

List of Tables xix

Chapter 1 – Introduction 1

1.1 Motivation 1

1.2 Objectives 2

Chapter 2 – Fundamentals of Magnetic Resonance 3

2.1 Spins 3

2.2 Larmor Precession 4

2.3 Excitation 5

2.4 Relaxation 6

  2.4.1 Longitudinal Relaxation 6

  2.4.2 Transverse Relaxation 7

2.5 Gradients 8

2.6 K-Space 9

2.7 Pulse Sequences 10

  2.7.1 Spin-Echo 11

  2.7.2 Inversion Recovery 12

  2.7.3 Gradient-Echo 13

2.8 T_1 and T_2 contrast 13

2.9 MR Spectroscopy 15

2.10 Functional MRI 17

2.11 Ultra-high magnetic field 19

Chapter 3 – Arterial Spin Labeling: An Overview 21

3.1 Perfusion 21

3.2 ASL – General Principles 21
3.3 Labeling strategies 22
  3.3.1 CASL – Continuous Arterial Spin Labeling 23
  3.3.2 PASL – Pulsed Arterial Spin Labeling 25
    3.3.2.1 PASL sequences 26
  3.3.3 PCASL – Pseudo-Continuous Arterial Spin Labeling 27
3.4 Quantification 27
3.5 fMRI – ASL versus BOLD 30
Chapter 4 – Methodology 33
4.1 Brief overview 33
4.2 Biological background 35
  4.2.1 Brain 35
  4.2.2 *Corpus Callosum* 35
  4.2.3 Visuo-Motor Interhemispheric Transfer 37
4.3 Sequences 38
  4.3.1 FAIRPRESS 38
  4.3.2 FAIRPRESS with background suppression 39
  4.3.3 PCASLPRESS 39
4.4 Participants 40
4.5 Experimental design 40
  4.5.1 Sequence Optimization 40
  4.5.2 Functional Studies 40
    4.5.2.1 Visual stimulus 41
    4.5.2.2 Adapted Poffenberger task 42
4.6 Data Acquisition 43
  4.6.1 Sequence Optimization 44
  4.6.2 Functional Studies 46
    4.6.2.1 Visual stimulus 47
    4.6.2.2 Adapted Poffenberger task (3T) 48
    4.6.2.3 Adapted Poffenberger Task (9.4T) 48
4.7 Postprocessing 49

  - 4.7.1 Sequence Optimization 50
    - 4.7.1.1 Reconstruction optimization 51
  - 4.7.2 Functional Studies 51
    - 4.7.2.1 T_2* reconstruction optimization 51

Chapter 5 – Sequence Optimization 53

5.1 FAIRPRESS optimization 53
  - 5.1.1 Reconstruction optimization 54
  - 5.1.2 Sequences 55

Chapter 6 – Functional Studies 59

6.1 General considerations 59

6.2 Visual stimulus 60
  - 6.2.1 T_2* reconstruction optimization 60
  - 6.2.2 Results 61

6.3 Adapted Poffenberger task (3T) 68
  - 6.3.1 T_2* reconstruction optimization 68
  - 6.3.2 Results 68

6.4 Adapted Poffenberger task (9.4T) 71
  - 6.4.1 Results 71

Chapter 7 – Conclusions and Future Work 75

References 77

List of Abbreviations

AFP – Adiabatic Fast Passage
ANOVA – Analysis of Variance
ASL – Arterial Spin Labeling
BOLD – Blood-Oxygen-Level Dependent
BS – Background Suppression
CASL – Continuous Arterial Spin Labeling
CBF – Cerebral Blood Flow
CBV – Cerebral Blood Volume
CC – *Corpus Callosum*
$CMRO_2$ – Cerebral Metabolic Rate of Oxygen
CNR – Contrast-to-Noise Ratio
CSF – Cerebral Spinal Fluid
CT – Computerized Tomography
DSC – Dynamic Susceptibility Contrast
DTI – Diffusion Tensor Imaging
EPI – Echo Planar Imaging
EPISTAR – Echo Planar Imaging and Signal Targeting with Alternating Radiofrequency
FAIR – Flow-sensitive Alternating Inversion Recovery
FID – Free Induction Decay
FLASH – Fast Low Angle Shot
fMRI – Functional MRI
FT – Fourier Transform
GE – Gradient Echo
GM – Grey Matter
HRF – Hemodynamic Response Function
IR – Inversion Recovery
MPRAGE – Magnetization Prepared Rapid Acquisition with Gradient Echo
MR – Magnetic Resonance
MRI – Magnetic Resonance Imaging
MT – Magnetization Transfer
MVS – Multi-Voxel Spectroscopy
OE – Oxygen Extraction
OVS – Outer Volume Suppression
PASL – Pulsed Arterial Spin Labeling
PCASL – Pseudo-Continuous Arterial Spin Labeling
PD – Proton Density
PET – Positron Emission Tomography
PICORE – Proximal Inversion with Control for Off-Resonance Effects
PRESS – Point Resolved Spectroscopy
RF – Radio-Frequency
ROI – Region of Interest
SE – Spin Echo
SNR – Signal-to-Noise Ratio
SPECT – Single-Photon Emission Computerized Tomography
STEAM – Stimulated Echo Acquisition Mode
SVS – Single-Voxel Spectroscopy
TA – Acquisition Time
TE – Echo Time
TI – Inversion Time
TIR – True Inversion Recovery
TR – Repetition time
TSE – Turbo Spin Echo
VC – Visual Cortex
WM – White Matter

List of Figures

Figure 1 – Left: In the absence of a magnetic field, the spins show a random orientation and the same energy level, cancelling each other, resulting in null magnetization. Right: In the presence of the magnetic field B_0, there is an energy gap and population difference between the parallel and anti-parallel states, generating macroscopic magnetization, parallel to B_0 [10]. 4

Figure 2 – In the presence of B_0, nuclei with non-zero spins precess around the direction of the field, just like the spinning top precesses around gravity (but with opposite directions of precession, since the external fields are opposite) [11]. 4

Figure 3 – The primary signal measured in MR, the FID. The signal decays approximately with a time constant T_2* due to both intrinsic T_2 decay and also dephasing due to magnetic field inhomogeneities [13]. 6

Figure 4 – Graphical representation of the longitudinal magnetization recovery and its T_1-dependent growth rate (adapted from [15]). 7

Figure 5 – Graphical representation of the transverse magnetization decay and its T_2-dependent decay rate (adapted from [15])... 8

Figure 6 – Association between the raw data (left) and its corresponding image data (right) [9]. 10

Figure 7 – SE sequence. Gs is turned on at the same time as the excitation pulse. It dephases the spins along the slice, which needs to be balanced with a gradient of opposite polarity and half the duration (the rephasing gradient). During the refocusing pulse, the gradient is switched on again so that only the spins of the previously stimulated slice are affected. Gp is then switched on briefly, so it imposes a different phase on the spins. The phase encoding steps on the diagram are represented by the multiple horizontal lines in the bar. During the SE, Gf is turned on. Since at the same time the echo is read out, this gradient is also called readout gradient [9]. 11

Figure 8 – The a) faster relaxing tissue and b) slower relaxing tissue will display the same grey value, due to the *TI* selected in this case (adapted from [9]). 12

Figure 9 – *TE* and T_2 contrast: for a short *TE* (A), there is almost no difference between the long and short T_2 tissues, but for larger *TE*s (B), the short T_2 tissue loses signal and becomes darker, while the long T_2 tissue remains brighter for a longer period [12]. 14

Figure 10 – *TR* and T_1 contrast: for a short *TR* (A), a tissue with a short T_1 regains most of its M_z, producing a large signal, while a tissue with long T_1 yields a small signal. For a long *TR* (B), this difference disappears due to the recovery of M_z in both tissues [12]. 14

Figure 11 – Axial brain image, showing suggested localization for a GM voxel (in the occipital midline) and for a WM voxel (in the parietal region) [19]. 16

Figure 12 – BOLD fMRI overview of the changes between basal and activated states [23]. 17

Figure 13 – Typical HRFs, for a short stimulus of approximately 1s (blue) and for a long stimulus of approximately 20s (red), measured with BOLD fMRI [24]. 18

Figure 14 – Motor activation measured by BOLD fMRI, fused with an anatomical image – 3D MPRAGE (Magnetization Prepared Rapid Acquisition with Gradient Echo) [26]..................... 19

Figure 15 – Diagram depicting CASL: pulse sequence (left) and relative positioning of the imaging and labeling regions (imaging region in red and labeling region in blue, on the right) (adapted from [18]). 23

Figure 16 – Spins magnetization variation (red) while flowing through the labeling plane (blue) (adapted from [33]). 24

Figure 17 – Diagram depicting PASL: pulse sequence (left) and relative positioning of the imaging and labeling regions (imaging region in red and labeling region in blue, on the right) (adapted from [18]). 25

Figure 18 – Pulsed ASL labeling schemes, depicting the labeling planes for EPISTAR (orange line) and FAIR (white line) [37]. 26

Figure 19 – Magnetization difference as a function of *TI* [41]. 28

Figure 20 – Flow chart describing the chronological evolution and optimization of the project. 34

Figure 21 – Left: Lateral view of the brain's division into lobes [48]. Right: Sagittal view of the brain, centered on the *corpus callosum*, its regions highlighted [47]. 35

Figure 22 – Sagittal view of a 3D reconstruction of all callosal fibers comprising bundles projecting into the prefrontal lobe (green), premotor and supplementary motor areas (light blue), primary motor cortex (dark blue), primary sensory cortex (red), parietal lobe (orange), occipital lobe (yellow), and temporal lobe (violet) [49]. 36

Figure 23 – Hofer's CC topography. Region I: prefrontal; region II: premotor and supplementary motor; region III: motor; region IV: sensory; region V: parietal, temporal, and occipital. A:anterior; P: posterior [49]. …………………………………………………………………….36

Figure 24 – FAIRPRESS sequence. Background suppression (grey), FAIR's perfusion encoding (red), slice selection only in tag scans (orange), outer volumes suppression (blue), PRESS volume selection (purple) and strong bipolar gradients (black). 38

Figure 25 – PCASLPRESS's labeling scheme (balanced PCASL). 39

Figure 26 – Still frame of the visual stimulus used.. 42

Figure 27 – Still frame of the visual stimulus used for the adapted Poffenberger task. 43

Figure 28 – PCASLPRESS's labeling plane, placed on the MPRAGE. Its positioning was based on PCASL's optimization studies found in the literature [56]. 43

Figure 29 – Voxel positioning on the CC, sagittal (MPRAGE), coronal and transverse views (localizer). 44

Figure 30 – Voxel positioning in grey matter, sagittal (MPRAGE), and transverse views (TSE). 45

Figure 31 – Voxel positioning on the ventricles, sagittal (MPRAGE), and transverse views (TSE). 45

Figure 32 – Transversal view of the voxel positioned on grey (left) and white (right) matter in the visual cortex (TSE). 47

Figure 33 – T_2*-weighted EPI results, acquired during the visual stimulus presentation. The significantly activated areas are superimposed on anatomical images. 48

Figure 34 – Voxel positioning in the CC. Sagittal (left) and transversal (right) views. 49

Figure 35 – Central points of the water spectra from the tagged (blue) and control (red) scans from a WM voxel. The difference between them is very small for WM, and slightly larger for GM. 50

Figure 36 – Relative magnetization difference in function of *TI*, measured in the CC for a single subject. 53

Figure 37 – Comparison between the three sequences for measurements in GM, regarding relative perfusion (left) and SNR (right). 55

Figure 38 – Comparison between the three sequences for measurements in white matter, regarding relative perfusion (left) and SNR (right). 56

Figure 39 – Relative perfusion comparison between the three sequences for measurements in the ventricle (left) and without perfusion labeling (right). 57

Figure 40 – Left: Data acquired during a measurement in the *corpus callosum*, with an outlier probably due to motion circled in red (Subject 5 in the Poffenberger Task experiments). Right: Same dataset, after outlier removal. 59

Figure 41 – Left: Perfusion and T_2* signals, acquired simultaneously for subject 1, in the GM. Above the graphics, the stimuli periods are represented in black and the rest periods in white. Right: Corresponding averaged data, where one point translates one state and also disregarding the points acquired during the activation delay considered for GM. 61

Figure 42 – Left: Perfusion and T_2* signals, acquired simultaneously for subject 8, in the CC. Above the graphics, the stimuli periods are represented in black and the rest periods in white. Right: Corresponding averaged data, where one point translates one state and also disregarding the points acquired during the activation delay considered for WM. 62

Figure 43 – Left: Perfusion and T_2* signals, acquired simultaneously for subject 6, in the VC. Above the graphics, the stimuli periods are represented in black and the rest periods in white. Right: Corresponding averaged data, where one point translates one state and also disregarding the points acquired during the activation delay considered for WM. 63

Figure 44 – Left: absFID reconstructed signal (blue) and the corresponding fit result (black). Right: complFID reconstructed signal (blue) and the corresponding fit result (black). Both graphs show background suppressed data from the same measurement in the CC. 68

Figure 45 – Left: Perfusion and T_2* signals, acquired simultaneously for subject 8, in the CC. Above the graphics, the stimuli periods are represented in black and the rest periods in white. Right: Corresponding averaged data, where one point translates one state and also disregarding the points acquired during the activation delay considered for WM. 69

Figure 46 – Left: Perfusion and T_2* signals, acquired simultaneously for subject 1, in the CC. Above the graphics, the stimuli periods are represented in black and the rest periods in white. Right: Corresponding averaged data, where one point translates one state and also disregarding the points acquired during the activation delay considered for WM. 72

List of Tables

Table 1 – Measured T_1 and T_2 values for white matter and grey matter, when subjected to a 3T B_0 [16]. 8

Table 2 – Summary of the comparison between ASL and BOLD when measuring neural activation (adapted from [8]). 31

Table 3 – Summarized experimental design for the activation experiments. 41

Table 4 – Summarized experimental design for the activation experiments. 46

Table 5 – Summarized experimental design for the activation experiments. 46

Table 6 – Mean intersubject SNR analysis for FAIRPRESS with background suppression, for the different reconstructions, in white matter. 54

Table 7 – One-Way ANOVA test results, for WM and GM and the different sequences. 54

Table 8 – Relative magnetization difference and SNR from the intersubject analysis, for the three sequences in GM. 55

Table 9 – Relative magnetization difference and SNR from the intersubject analysis, for the three sequences in WM. 56

Table 10 – Mean intersubject SNR analysis for FAIRPRESS without BS, for the two reconstructions, in the CC and only for the rest state. 60

Table 11 – Student's t-test results for the different subjects in grey matter. 64

Table 12 – Student's t-test results for the different subjects in the CC. 65

Table 13 – Student's t-test results for the different subjects in the WM of the VC. 66

Table 14 – Student's t-test results for subject 1 in grey matter. 69

Table 15 – Student's t-test results for the different subjects in the CC. 70

Table 16 – Student's t-test results for subject 1 in GM. 71

Table 17 – Student's t-test results for both subjects in the CC. 72

Chapter 1
Introduction

1.1 Motivation

Arterial Spin Labeling (ASL) has become a valuable tool for measuring cerebral perfusion in grey matter (GM) over the last years. However, detecting focal changes in white matter (WM) perfusion is challenging and represents a great disadvantage of ASL over PET (Positron Emission Tomography). In WM, perfusion tends to be much lower than in GM, which limits the signal-to-noise ratio (SNR) of ASL measurements. The transit time of WM is also considerably larger than in GM, which means there is more longitudinal relaxation of the labeled spins of interest. Precise knowledge of the tissue transit time of blood is more important for accurate perfusion quantification in WM. SNR in deep WM perfusion has been previously measured to be less than 1 using the FAIR (Flow-sensitive Alternating Inversion Recovery) sequence [1].

However, recent developments in ASL sequences have improved the detection of WM perfusion. Some years ago, PCASL (Pseudo-Continuous ASL) was used to investigate the number of averages necessary to obtain accurate single post-label delay time images and their effect on WM contrast-to-noise ratio (CNR) [2], and multiple post-labeling delay PCASL acquisition was combined with fine detail ROI (Region of Interest) analysis [3], both yielding promising results for measuring WM perfusion.

The technique used in this project, based on the combination of pulsed ASL FAIR acquisition with single-voxel spectroscopic localization (PRESS) – the FAIRPRESS sequence – has already been successful in measuring perfusion values both in WM and in rat skeletal muscle [4, 5].

Over the past 20 years a great number of BOLD (Blood-Oxygen-Level Dependent) fMRI (functional Magnetic Resonance Imaging) studies have been published, however, only a very small number of these studies report WM activation. Since WM corresponds to approximately half of the brain tissue, this discrepancy takes larger proportions. Low magnitude of the signal in WM, mainly due to its lower cerebral blood flow (CBF) and cerebral blood volume (CBV), a possibly different Hemodynamic Response Function (HRF) for WM activation, and artifacts caused by motion, partial voluming effects and physiological noise, might be some of the reasons behind it [6]. The source of the BOLD fMRI signal has also been mainly associated with post-synaptic potentials, the majority of which occur in GM [7].

Even so, studies reporting WM activation have seen a recent increase. The majority of these studies has been performed on the *corpus callosum* (CC) and relied on interhemispheric tasks, which involve hemi-field presentation of visual stimuli and motor responses from either the hand on the same side of the presented stimulus, or in the opposite side, in order to activate the CC. Besides choosing the appropriate task, the signal acquired from WM can also be enhanced by applying higher magnetic field strengths and using MRI sequences that have this tissue's particularities in mind [6].

Functional studies with ASL have shown better spatial localization than BOLD, also allowing for absolute quantification of perfusion changes with activation. The combination of BOLD with ASL can also be performed, to measure changes in oxygen related to activation and increase our knowledge about the formation of BOLD signal changes [8].

Thus, being able to reliably measure absolute quantitative perfusion values in WM during rest and to detect perfusion changes during activation would be of great interest for the identification of WM dysfunction and open new neuroscience research routes in the future, regarding brain mapping and brain connectivity.

1.2 Objectives

The main goals of this thesis were as follows:

- Optimization of FAIRPRESS sequence parameters;
- Evaluation of FAIRPRESS, PCASLPRESS and FAIRPRESS with background suppression;
- Optimization of the reconstruction routines;
- Stimulus improvement;
- Simultaneous measurement of perfusion and BOLD during activation, in the *corpus callosum* and in both grey and white matter in the visual cortex, using a 3T magnetic field;
- Simultaneous measurement of perfusion and BOLD during activation, in the *corpus callosum* and in grey matter in the visual cortex, using a 9.4T magnetic field.

Chapter 2

Fundamentals of Magnetic Resonance

Magnetic Resonance Imaging (MRI) is an essential tool in modern medical imaging, combining strong magnetic fields and radio-frequency (RF) signals to create pictures of tissues, organs and structures inside the body. The present chapter introduces some of the concepts associated with this technique.

2.1 Spins

The human body contains a large number of atoms. Atomic nuclei with an odd-number of protons and neutrons have an associated spin, their intrinsic angular momentum. Hydrogen nuclei are the most commonly used in Magnetic Resonance (MR) studies because ^{1}H is the most abundant atom in the human body, being present in every water molecule, and also because it contains a single proton, making it easy to model.

Each hydrogen proton behaves like a small magnet. While in a field-free space, the local magnetic fields of these protons are randomly oriented and cancel each other out. Therefore, the bulk magnetization ($\mathbf{M}$), the vector sum of all spin magnetic moments, will typically be zero.

However, when subjected to a magnetic field like $\mathbf{B}_0$ inside the MRI system, the spins tend to align parallel or anti-parallel to the applied field. The parallel orientation corresponds to a lower energy state, making it slightly more prevalent than the anti-parallel state [9]. This energy splitting into multiple discrete energy states in the presence of a static magnetic field is called the Zeeman Effect [10]. Spatial addition of the non-canceled spins is what generates the macroscopic magnetization effect that is measured in MRI acquisitions.

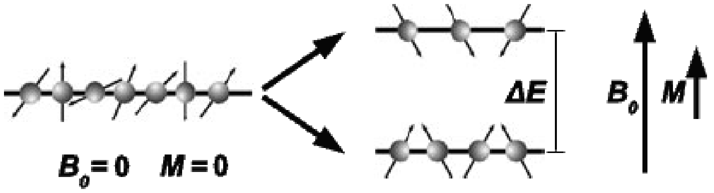

Figure 1 – **Left**: In the absence of a magnetic field, the spins show a random orientation and the same energy level, cancelling each other, resulting in null magnetization. **Right**: In the presence of the magnetic field $\mathbf{B}_0$, there is an energy gap and population difference between the parallel and anti-parallel states, generating macroscopic magnetization, parallel to $\mathbf{B}_0$ **[10]**.

2.2 Larmor Precession

In the same manner as a spinning top precesses around the axis defined by gravity, a spin subjected to a magnetic field rotates in the shape of a cone, around the direction of the applied field – the spin precession (Fig. 2).

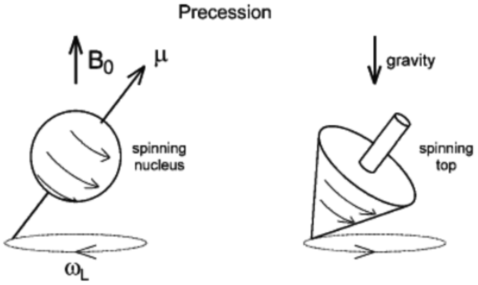

Figure 2 – In the presence of $\mathbf{B}_0$, nuclei with non-zero spins precess around the direction of the field, just like the spinning top precesses around gravity (but with opposite directions of precession, since the external fields are opposite) **[11]**.

The frequency of this movement is constant and depends only on the type of the nucleus and the strength of the applied magnetic field, as described in Equations 1 and 2.

$$\omega_0 = \gamma B_0 \qquad \textbf{Equation 1}$$

or

$$v_0 = \frac{\gamma}{2\pi} B_0. \qquad \textbf{Equation 2}$$

In these equations, B_0 is the strength of the external magnetic field, γ is the gyromagnetic ratio of the nuclei (depends solely on the type of nucleus), ω_0 is the angular velocity of this movement and v_0 is the Larmor frequency – the precession frequency [10].

2.3 Excitation

The bulk magnetization is very small when compared to the external magnetic field (Fig.1). Its magnitude is less than the Earth's magnetic field, making it nearly impossible to measure when aligned with $\mathbf{B}_0$ in the z-axis. However, by tilting **M** from the z-axis, it will precess and originate a component in the xy-plane that can then be measured.

This is done by applying an additional rotating magnetic field with lower amplitude than B_0, designated $\mathbf{B}_1$, which is turned on for a short period of time perpendicularly to $\mathbf{B}_0$, in effect generating a RF pulse, so called due to the usual frequencies involved (several MHz). If this field oscillates at the same frequency as the Larmor frequency of the spins, it will interfere with the spins' equilibrium by a process of resonant excitation. The excess spins that were aligned with $\mathbf{B}_0$ will then precess in synchrony, tipping the magnetization **M** from the longitudinal direction and producing a component in the transverse plane [11].

We can then differentiate between longitudinal magnetization ($\mathbf{M}_z$) – the portion of the bulk magnetization vector **M** in the z-direction, along $\mathbf{B}_0$ and transverse magnetization ($\mathbf{M}_{xy}$) – the component of the **M** vector that rotates in the x-y plane.

When the $\mathbf{B}_1$ field is turned off, the transverse magnetization continues to precess at the Larmor frequency. According to Maxwell-Faraday's equation, this time-varying magnetic field will induce a small electric voltage in the receiver RF-coil. This current over time is the MR signal, called the Free Induction Decay (FID), which also oscillates with ω_0 and falls off exponentially as described by Eq. 3 and represented in Fig. 3 [12].

$$S(t) = S_0 . cos(\omega_0 t) . e^{-\frac{t}{T_2^*}} \qquad \textbf{Equation 3}$$

S_0 is the initial signal amplitude and T_2^* is the apparent transverse relaxation time, which will be explained in more detail in another section of this thesis [10].

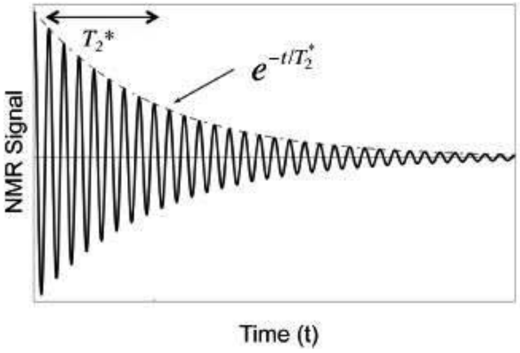

Figure 3 – The primary signal measured in MR, the FID. The signal decays approximately with a time constant T_2* due to both intrinsic T_2 decay and also dephasing due to magnetic field inhomogeneities **[13]**.

The stronger the energy of the excitation pulse and the longer its duration, the farther the **M** vector will tilt. The final tilt angle is called the flip angle (α). An RF pulse with α=90º will flip the magnetization into the xy-plane, while a pulse of α=180º will flip the magnetization into the opposite direction of the z-axis (this is also called an inversion pulse, since it inverts the direction of the magnetization) [14].

2.4 Relaxation

After an RF pulse disturbance, the spins return to their equilibrium state by a process of relaxation. This has to be described by two independent processes, separating both the transverse and longitudinal magnetizations; while $\mathbf{M}_z$ is recovering, $\mathbf{M}_{xy}$ is decaying, this decay being faster than the $\mathbf{M}_z$ recovery.

2.4.1 Longitudinal Relaxation

T_1 indicates how quickly a spin ensemble is able to transmit its excess energy to the lattice (the surroundings of the proton). It is the time needed for the longitudinal magnetization to return from zero to about 63% of its original magnitude, after the RF pulse is turned off. After ~5T_1, M_z is almost fully recovered.

In *in vivo* experiments, its value is in the order of seconds [10]. The T_1 tends to be longer in body fluids, like blood or cerebrospinal fluid (CSF), than in more solid tissues, like WM in the brain. Since this relaxation is caused by interactions with the surroundings of the nuclei, the T_1 value depends on both the type of tissue and also on which molecule the nucleus is bound to. This T_1 tissue specificity is fundamental in obtaining sharp image contrast in MRI.

Assuming the initial value of M_z is null (after a 90º RF pulse, for simplicity), its recovery is given by Eq. 4, and is described in Fig. 4.

$$M_z(t) = M_0(1 - e^{\frac{-t}{T_1}}) \quad \textbf{Equation 4}$$

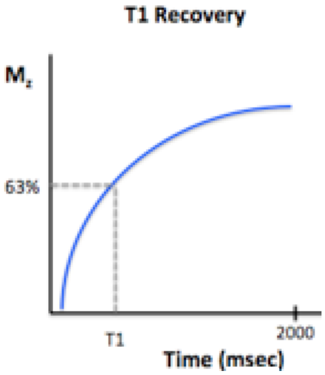

Figure 4 – Graphical representation of the longitudinal magnetization recovery and its T_1-dependent growth rate (adapted from **[15]**).

2.4.2 Transverse Relaxation

T_2 is the time constant in transverse relaxation. The T_2 decay is about 5 to 10 times shorter than the T_1 relaxation. Immediately after the RF pulse the spins are phase-coherent, but eventually they begin to lose coherence due to interactions with magnetic fields from the individual nuclei, dephasing amongst themselves and causing the decay of the transverse magnetization due to loss of coherence. After a time T_2, M_{xy} has lost 63% of its value before relaxation. *In vivo*, this time constant is measured in milliseconds [10]. This magnetization decay is described by Eq. 5 and is represented in Fig. 5.

$$M_z(t) = M_0 . e^{\frac{-t}{T_2}} \quad \textbf{Equation 5}$$

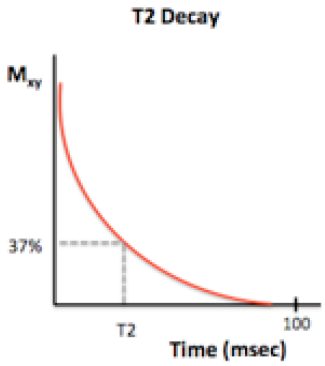

Figure 5 – Graphical representation of the transverse magnetization decay and its T_2-dependent decay rate (adapted from **[15]**).

In practical terms, however, this decay is much faster. Due to additional dephasing caused by field inhomogeneities (small differences in the local field at different locations, either because of technical inhomogeneities of the magnet or even inhomogeneities in the subject's body), that cause destructive interference and shortening of the FID. This effective decay of the FID also has an associated time constant, called T_2*, previously presented in Fig. 3, which is always shorter than T_2 [9].

Even though typical values for the time constants were previously mentioned, they vary widely between different tissues (and also for different B_0s), as depicted in Table 1.

Table 1 – Measured T_1 and T_2 values for white matter and grey matter, when subjected to a 3T B_0 **[16]**.

Tissue	T_1 (ms)	T_2 (ms)
WM	832	110
GM	1331	80

2.5 Gradients

To be able to differentiate between locations and form images from these signals, the precession frequency must change with position so that a receiver can "tune" to a location. Since the precession frequency is proportional to field strength (Eq. 1), this is achieved by applying field gradients, using three pairs of gradient coils along the x, y and z axis that produce linear spatial variations along the magnetic field [14].

For slice-selection, a gradient pulse is turned on in the z-direction simultaneously to the RF pulse, called the slice-selection gradient (Gs). Due to the spatial variation in the magnetic field, only spins in a region perpendicular to the gradient – the slice – will be excited, as the resonant frequencies will be impacted by the presence of Gs. Its thickness can be altered by either modifying the bandwidth of the RF pulse or by changing the gradient strength. The spins outside the slice are not affected by the RF pulse, so the MR signal is only generated within the selected region.

Along the x-direction, the signals from different locations can be differentiated by switching a gradient in the x-axis. The spins will then precess along the axis with increasing frequency. This is called frequency-encoding, and the gradient used is the frequency-encoding gradient (Gf).

Between the RF pulse and the echo acquisition window, the gradient in the y-axis is switched on briefly, causing the spins to precess at different speeds for a short time. When the gradient is turned off, they will have different phases, related to their locations. This is phase-encoding, and the gradient used is the phase-encoding gradient (Gp). Since one Gp can only phase-modulate one line of k-space (see below, section 2.6), phase-encoding requires several scans. Each scan line will have a different Gp strength, imposing spatially dependent phase-shifts between the signals. More phase-encoding steps improve resolution and image quality, but also prolong the scan time [9, 12].

2.6 K-Space

The data from the previously mentioned encoding steps is collected in a spatial-frequency space, called k-space. Its horizontal axis (k_x) represents the frequency information and the vertical axis (k_y) the phase information. A single slice corresponds to a plane in the k-space. A dot in the k-space raw data does not correspond directly to a pixel of the image, but each dot has information about frequency, phase and signal intensity.

The raw data in the center determines the image contrast and rough structures, while the raw data in the periphery contains information about margins, contours and finer structures, and is responsible for defining resolution [17].

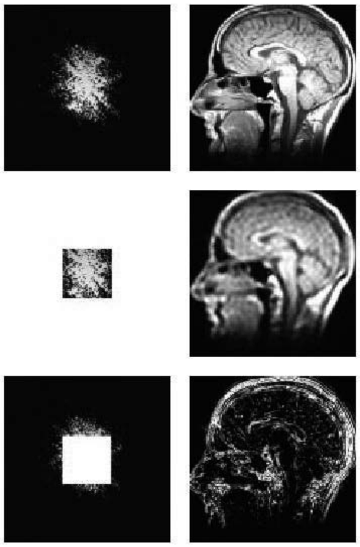

Figure 6 – Association between the raw data (**left**) and its corresponding image data (**right**) **[9]**.

By applying the Inverse Fourier Transform, the raw data values in k-space are used to calculate the grey value distribution in the image, associating it to each pixel and reconstructing the raw data. Each pixel in the resulting image is the weighted sum of all the individual points in k-space, meaning that any disturbance in k-space data translates into a distortion in the image, determined by the phase and frequency data stored in that point (Fig. 6) [17].

2.7 Pulse Sequences

A basic pulse sequence includes RF pulses, slice-selection, frequency-encoding and phase-encoding gradients, and also the read-out of the FID signal.

The pulse sequence is repeated with TR (repetition time), the time between two consecutive excitation pulses. The number of phase-encoding steps (*Np*), which corresponds to raw data lines in k-space, is the number of repetitions of the sequence. The *TA* (acquisition time) is then given by Eq. 6.

$$\boldsymbol{TA = Np \times TR} \qquad \textbf{Equation 6}$$

The echo time (*TE*) is the time between the excitation pulse and the peak of the generated echo, when the MR signal is sampled. This concept of "echo" is described in detail in section 2.7.1, below.

MR techniques strongly depend on choosing the adequate pulse sequence and acquisition parameters [9].

2.7.1 Spin-Echo

Spin-echo (SE) sequences use a slice-selective 90° RF pulse for excitation, after which the transverse magnetization decays with T_2*. After half of the *TE* has passed, a 180° RF pulse is applied to refocus the spins: the rotation direction is the same, but the magnetization is flipped around the transverse plane. The spins that were ahead before are now behind and vice-versa. However, the spins that are now behind will draw near since they are still exposed to the same field inhomogeneities, which caused the phase differences in the first place. After the second half of the *TE*, all the spins meet once again in phase, generating the SE.

The 180º refocusing pulse consequently eliminates the effects of static magnetic field inhomogeneities, but it cannot compensate for spin-spin interactions. Therefore, the magnetization decay that occurs after excitation depends only on the spin-spin interactions, decaying with T_2 rather than T_2*, making it insensitive to static field inhomogeneities, which is one of the great advantages of this technique [9, 12].

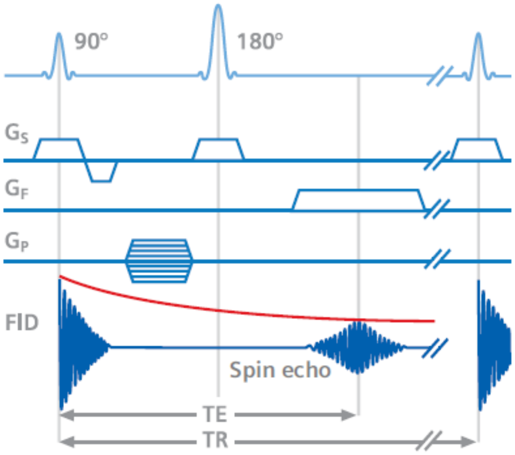

Figure 7 – SE sequence. Gs is turned on at the same time as the excitation pulse. It dephases the spins along the slice, which needs to be balanced with a gradient of opposite polarity and half the duration (the rephasing gradient). During the refocusing pulse, the gradient is switched on again so that only the spins of the previously stimulated slice are affected. Gp is then switched on briefly, so it imposes a different phase on the spins. The phase encoding steps on the diagram are represented by the multiple horizontal lines in the bar. During the SE, Gf is turned on. Since at the same time the echo is read out, this gradient is also called readout gradient **[9]**.

2.7.2 Inversion Recovery

The inversion recovery (IR) sequence adds a preparation pulse of 180º before the spin-echo, inverting $\mathbf{M}_z$. $\mathbf{M}_{xy}$ remains zero, so there is no signal after the inversion pulse. The time interval between the inversion pulse and the excitation pulse is called the inversion time (*TI*). During *TI*, $\mathbf{M}_z$ recovers. A 90º excitation pulse then converts the current $\mathbf{M}_z$ into $\mathbf{M}_{xy}$.

After the inversion, $\mathbf{M}_z$ relaxes its negative value, so that the **M** of different tissues reaches zero at different times. By changing the *TI*, the image contrast can be manipulated. With a short *TI*, all negative $\mathbf{M}_z$ is flipped into the xy-plane. With a longer *TI*, less longitudinal magnetization flips to the transverse plane, generating a weaker signal. However, if *TI* is long enough to allow full relaxation, the signal becomes stronger again [9, 12].

When only the signal magnitude is used for image contrast, and there are tissues with different relaxation speeds, there may be no differentiation made between positive and negative M_z. Therefore, tissues with very different T_1s may be represented with the same grey value. Signals from white or grey matter may even disappear, depending on the *TI* used.

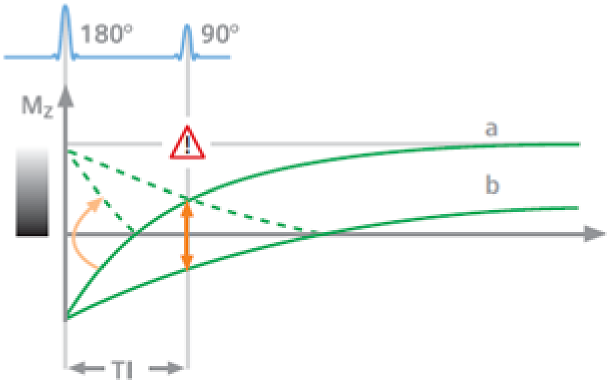

Figure 8 – The a) faster relaxing tissue and b) slower relaxing tissue will display the same grey value, due to the *TI* selected in this case (adapted from **[9]**).

This problem can be solved by considering $\mathbf{M}_z$'s orientation. By taking into account not only the magnitude but also the phase of the signals, it is possible to differentiate the signals with originally positive or negative $\mathbf{M}_z$, ensuring maximum T_1 contrast. This phase-sensitive reconstruction technique is called True Inversion Recovery (TIR) [9, 10, 12].

2.7.3 Gradient-Echo

As the name suggests, gradient-echo (GE) sequences use the gradient coils to generate an echo, instead of pairs of RF pulses. By first applying a frequency-encoding gradient with negative polarity to destroy the phase coherence of the precessing spins (dephasing), the gradient is then reversed and the spins rephase to generate a GE.

The applied excitation pulse has a flip angle lower than 90º. This means the effect of the whole available magnetization in the transverse plane will not be present, rather only a part of it is converted to $\mathbf{M}_{xy}$. Nonetheless, $\mathbf{M}_z$ still has a small magnitude, meaning that for the following pulse there is still M_z "available", allowing for very short *TR*s. As *TR* is a major determinant of the overall *TA*, much faster imaging is possible when compared with SE and IR sequences, which is the most important advantage of this sequence [9, 10, 12].

2.8 T_1 and T_2 contrast

TE and *TR* are very important parameters when controlling contrast. By choosing a sufficiently long *TR*, the difference in signal after a repetition of the RF pulse will depend mainly on the proton density (PD) of the tissue, due to the almost complete longitudinal relaxation. By also generating echoes shortly after the RF pulses, with short *TE*s, we obtain a PD-weighted image.

If besides selecting a long *TR*, a long *TE* is also selected, we can see that at longer echo times the M_{xy} curves begin to diverge (Fig. 9), so the contrast will be controlled by T_2 relaxation – the resulting image will be T_2-weighted.

The T_2 contrast depends strongly on the selected *TE*. Its optimal value is the mean value of the T_2 constants of the tissue of interest. However, if the *TE* is too long, M_{xy} decays to such a level that the signal of some types of tissue disappears in the signal noise.

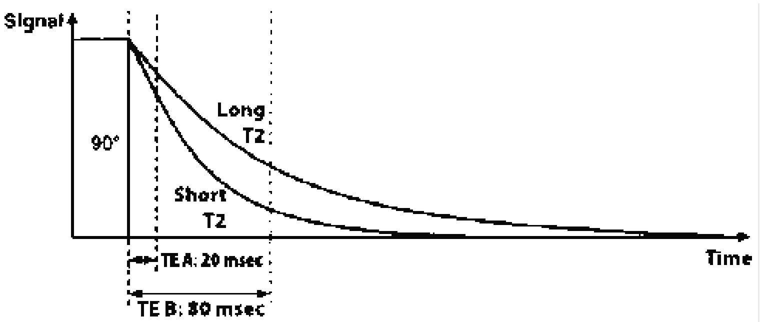

Figure 9 – *TE* and T_2 contrast: for a short *TE* (A), there is almost no difference between the long and short T_2 tissues, but for larger *TE*s (B), the short T_2 tissue loses signal and becomes darker, while the long T_2 tissue remains brighter for a longer period **[12]**.

By selecting a short *TR*, T_1 relaxation is not complete, and the signals will be much weaker, so the smallest possible *TE*s must also be chosen. The short *TR* cancels the effect of PD, and the short *TE* cancels the effect of T_2 relaxation, so the image obtained depends mainly on the T_1 relaxation of the tissue – a T_1 weighted image is acquired.

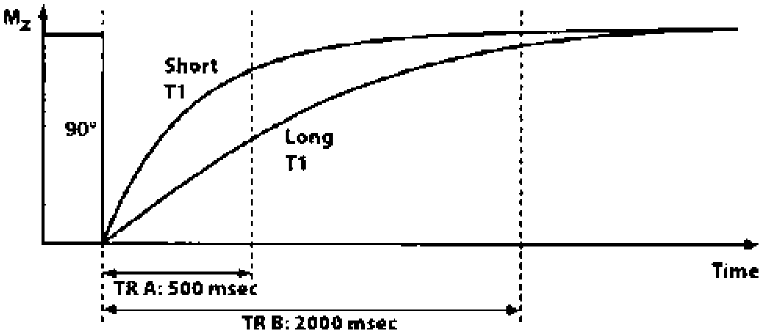

Figure 10 – *TR* and T_1 contrast: for a short *TR* (A), a tissue with a short T_1 regains most of its $\mathbf{M}_z$, producing a large signal, while a tissue with long T_1 yields a small signal. For a long *TR* (B), this difference disappears due to the recovery of $\mathbf{M}_z$ in both tissues **[12]**.

Soft tissues have only small differences in PD, but have different T_1 relaxations, which makes T_1-weighted imaging ideal for anatomical displays.

In MR scans, tissues with longer T_1 appear darker in a T_1-weighted image, while tissues with larger T_2 appear brighter [9, 12].

2.9 MR Spectroscopy

By using a single Fourier Transform (FT), the FID can be converted from the time to the frequency domain, in order to analyze its spectrum.

If the signal has only one frequency (sine oscillation) the associated spectrum will have a single resonance line for the associated frequency. Since the signal decreases and has a bandwidth, the resonance line changes into a peak of limited width. This peak represents the resonance frequency in the measured voxel, and the area under the peak is proportional to the signal emitting nuclei.

Hydrogen atoms are bound to different molecules and to different positions. This leads to variations in the local magnetic field, and also in the resonance frequencies of the bound protons when compared to Larmor frequencies. This change in resonance frequencies is called the chemical shift. This is the reason why the nuclei of a molecule can have multiple resonance lines. In the spectrum, the chemical shift can be visualized as a shift of the associated resonance lines or peaks, which allows us to differentiate between substances, molecules and molecular components [9].

This technique can be performed by two different methods: Single Voxel Spectroscopy (SVS), or Multi Voxel Spectroscopy (MVS):

- In MVS, spectra are obtained from multiple voxels of interest, in a single slab of tissue. When compared to SVS, a much larger area can be covered, almost eliminating the sampling error, but it presents the disadvantage of lower SNR and longer *TA*;
- In SVS a single volume of interest is selected, by using the intersection of three mutually orthogonal slabs, where each slab is excited by a spatially selective pulse in the presence of a gradient. A single spectrum is then obtained from the voxel of interest [18].

SVS provides better SNR and is more robust than MVS, but only one spectrum is obtained. The choice of voxel positioning is then of critical importance and it may lead to interpretation errors if not done properly. An example of good voxel placement in GM and WM is depicted on Fig. 11. Suitable contrast images are also needed for good positioning [19, 20].

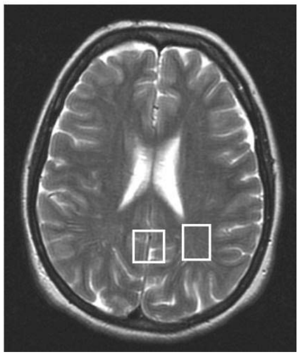

Figure 11 – Axial brain image, showing suggested localization for a GM voxel (in the occipital midline) and for a WM voxel (in the parietal region) **[19]**.

Two sequences are mainly used for single voxel MRS:

- Stimulated Echo Acquisition Mode (STEAM) uses a stimulated echo generated by three 90° pulses, each with a gradient on one of the three axes. There may be signal loss due to motion sensitivity at long *TE*s. This method is then more suitable for short *TE* acquisitions;
- Point Resolved Spectroscopy (PRESS) uses a double spin echo scheme, with a 90º pulse followed by two 180º pulses, where each pulse has a slice-selective gradient on one of the three main axes so that only the protons within the voxel experience the three RF pulses. This sequence gives better SNR than STEAM, so spectra can be acquired in a shorter period of time. It is more fitting when there is interest in small volumes [21].

2.10 Functional MRI

Functional magnetic resonance allows for *in vivo* measurements of brain activity. Even though magnetic susceptibility effects can cause artifacts when imaging the brain, they are the basis for the most popular technique for functional MR – BOLD fMRI.

The basis of this method is that the magnetic state of hemoglobin depends on its oxygenation. Deoxygenated hemoglobin is paramagnetic, while oxygenated hemoglobin is diamagnetic, relatively to brain tissue [22].

Deoxyhemoglobin tends to reduce the local MR signal by slightly dephasing the spins of the hydrogen nuclei in proximal water molecules of blood vessels and the adjacent tissue, creating small field gradients that lead to destructive interference and shortening of the T_2* relaxation time. Therefore, a drop in deoxyhemoglobin will originate a longer T_2* and a slight increase in the MR signal.

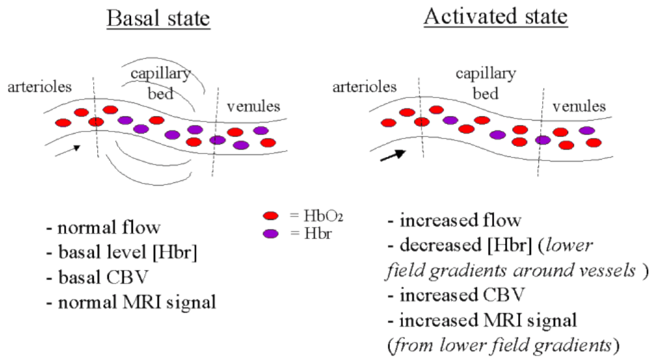
Basal state
Activated state
arterioles
capillary bed
venules
arterioles
capillary bed
venules
- normal flow
- basal level [Hbr]
- basal CBV
- normal MRI signal
● = HbO2
● = Hbr
- increased flow
- decreased [Hbr] (*lower field gradients around vessels*)
- increased CBV
- increased MRI signal
(*from lower field gradients*)

Figure 12 – BOLD fMRI overview of the changes between basal and activated states **[23]**.

BOLD does not reflect a single physiological process, but rather the combined effects of CBF, cerebral metabolic rate of oxygen ($CMRO_2$) and CBV [22]. An increase in neuronal activation in the brain leads to an increase in CBF (Fig. 12). This increase is approximately twice as large as the $CMRO_2$'s [24]. This imbalance translates into a decrease of the local oxygenation extraction fraction (OE) with activation. Since the local blood is more oxygenated, there is less deoxyhemoglobin present, slightly increasing the MR signal. The observed signal is then a composition of different signals related to different neural events.

This signal, also called the HRF, is complex, and is typically delayed by 1 to 2s in the GM, due to the vascular system's delayed response to the brain's need for glucose. It reaches its maximum between 5 and 10s. An initial dip of the signal can sometimes be seen. After the stimulus ends, a post-stimulus overshoot is often present, lasting typically 20s or more, after which the signal returns to the baseline (Fig. 13) [24].

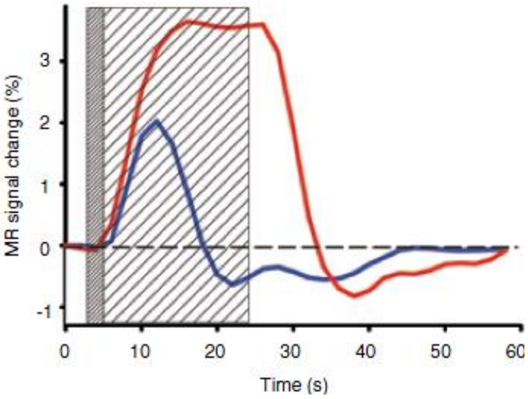

Figure 13 – Typical HRFs, for a short stimulus of approximately 1s (blue) and for a long stimulus of approximately 20s (red), measured with BOLD fMRI **[24]**.

The characteristics of the HRF vary between different brain regions and depend on the stimulus and its duration [25].

Brain activation studies usually use an experimental paradigm in which a subject alternates between periods of stimulation and rest, while a rapid series of MR images are acquired: this is called a block design. The time series of each image voxel is then analyzed, to determine if the signal shows correlation with the stimulus (i.e. if it increases in the presence of the stimulus and decreases with rest). The pixels that show correlation are then displayed in color on a regular anatomical MR image, as the areas activated by the stimulus (Fig. 14) [24].

Since the T_2* decay is very fast, there are only 100ms to generate the echoes. EPI (Echo-Planar Imaging) is currently the fastest MR imaging technique, being the preferred method for these measurements. It is a single shot method, meaning that it requires a single excitation pulse in order to acquire an entire image. The readout gradient is switched bipolarly, by generating a series of ascending and descending gradient echoes with alternate polarity, within the course of one FID. Due to its very fast acquisition, EPI is very robust to motion artifacts, therefore being the preferred method for diffusion, cranial perfusion and functional neuroimaging. However, since it has a long acquisition per excitation, it is also very susceptible to $\mathbf{B}_0$ inhomogeneities.

Since EPI is only a readout module, it can be combined with other preparation pulses (IR, SE or others), allowing us to obtain different kinds of contrasts with this technique [9].

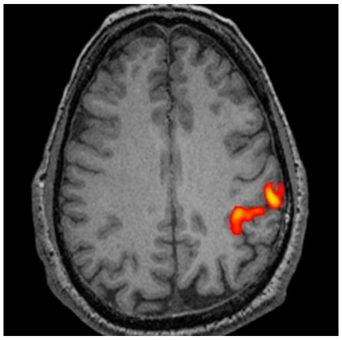

Figure 14 – Motor activation measured by BOLD fMRI, fused with an anatomical image – 3D MPRAGE (Magnetization Prepared Rapid Acquisition with Gradient Echo) **[26]**.

2.11 Ultra-high magnetic field

At higher magnetic field strengths, a higher proportion of the spins align parallel to the field, resulting in higher SNR. The higher magnetic field strength also influences the way the spins interact with each other and with the lattice, resulting in longer T_1 relaxation times and shorter T_2 decay times. The CNR of T_2-weighted images can thus be increased. Therefore, ultra-high magnetic fields can have increased sensitivity, contrast and resolution, improving the study of the function and structure of the brain [27].

However, as the magnetic field strength increases, higher frequency RF pulses are required to excite the bulk magnetization into the transverse plane, resulting in tissue heating due to RF power deposition. Another physiological issue that limits using ultra-high field strengths for human MRI is subject movement inside the $\mathbf{B}_0$ field, which may cause stimulation of sensory afferents of the central nervous system. This might result in temporary metallic taste or vertigo and nausea, which is more common with increasing field strengths [27]. While high fields offer the possibility of improved image quality, the safety and comfort of human subjects must be ensured.

In addition, it is more difficult to create and maintain a homogeneous static field when the field strength is higher and more susceptible to inhomogeneities produced by introducing a subject in the field. Perturbations in the magnetic field are linearly dependent on $\mathbf{B}_0$, making the shimming of the magnet for each scan at higher field strengths extremely important [27].

Chapter 3

Arterial Spin Labeling: An Overview

Arterial Spin Labeling is an MRI technique that allows for noninvasive perfusion quantification, by magnetically labeling water in arterial blood and using it as a tracer. It has been greatly improved over the last years, making it a very promising method. The main ideas behind it are presented in this chapter.

3.1 Perfusion

Perfusion is the delivery of oxygen and nutrients to the tissue by means of blood flow. It is classically measured using a diffusible tracer that can exchange between the vascular compartment and tissue [28].

The brain is highly perfused, receiving approximately 20% of the cardiac output, which reflects its high metabolic rate even at rest. It also has a well defined arterial supply, making it a good organ for perfusion measurements. The amount of blood that is supplied to the brain is expressed as CBF [18]. Perfusion is measured in milliliters of blood flow, per gram of tissue, per unit of time [ml/g/min].

The most commonly used techniques in current clinical practice use contrast agents as tracers to image CBF, like gadolinium-based contrast agents in Dynamic Susceptibility Contrast MRI (DSC-MRI), or iodine based contrast agents in Computerized Tomography (CT) perfusion imaging. However, there are concerns regarding the negative effects of ionizing radiation in general, and also regarding the use of contrast agents in patients with bad renal function: the latter is further limited by the need for intravenous access in infants and children [29].

3.2 ASL – General Principles

Arterial Spin Labeling uses magnetically labeled endogenous blood water as a tracer for perfusion MRI. It was first introduced in 1992 by Williams and Detre for visualizing brain perfusion and quantifying CBF [30]. By applying RF pulses, the $\mathbf{M}_z$ of arterial blood water is manipulated in a way that it differs from the magnetization of the tissue.

The general procedure of this technique is as follows: after an initial RF labeling phase, during which the flowing magnetization is tagged by saturation or inversion, there is a delay to allow the labeled protons to flow through the vascular tree and reach the tissue of interest. Then, an imaging pulse sequence is applied, and the tagged image is acquired. This procedure is then repeated, this time without labeling, to acquire a control image. The perfusion contrast is then given by the small difference between the tagged and the control images, caused by the exchange of labeled blood water molecules from blood to the surrounding tissue. The subtraction between the two images removes the static tissue signal. The magnetization difference is about 1% of M_0, the reference magnetization acquired before applying any pulses. A model can then be applied in order to obtain a calculated CBF image, showing a quantitative perfusion value for each voxel [28].

This technique has been shown to have many advantages:

- Gives absolute perfusion values, by using an endogenous tracer;
- Can be repeated almost unlimitedly, since it is non-invasive (does not require the injection of a contrast medium) and non-radioactive (it decays with T_1 relaxation);
- Makes it possible to measure normal physiology and its variations with time;
- Has a greater spatial resolution than PET/SPECT (radiation based imaging methods).

However, it also presents some issues:

- The duration of each measurement is relatively long;
- Has low SNR, and the fast decay time of the tracer may result in having little remaining signal when the blood reaches the tissue;
- Cannot be used in low blood flow situations or pathologies.

The future development of higher magnetic fields for MRI will benefit this technique, increasing its SNR. Quantitative functional perfusion MRI will eventually replace some BOLD fMRI studies (as per its dependency on CBF, as seen above in section 2.10) [18].

3.3 Labeling strategies

ASL has two main labeling strategies: Continuous Arterial Spin Labeling (CASL) and Pulsed Arterial Spin Labeling (PASL). Recently, an intermediate labeling technique has been introduced called Pseudo-Continuous Spin Labeling (PCASL) [31].

3.3.1 CASL – Continuous Arterial Spin Labeling

CASL was the first implementation of ASL. Low-power pulses with duration of 1 to 2s are continuously applied in presence of a gradient, on a plane inferior to the brain, inverting the blood magnetization (Fig. 15). This blood then flows into the brain, creating a steady-state where the regional brain magnetization reaches a new equilibrium governed by CBF. In humans, the labeling plane needs to be inferior to the Circle of Willis, where the major feeding arteries of the brain are perpendicular to the tagging plane. For slice selection, the long RF pulses are applied off-resonance and in the presence of a slice-selective gradient, along the flow direction in the arteries [31].

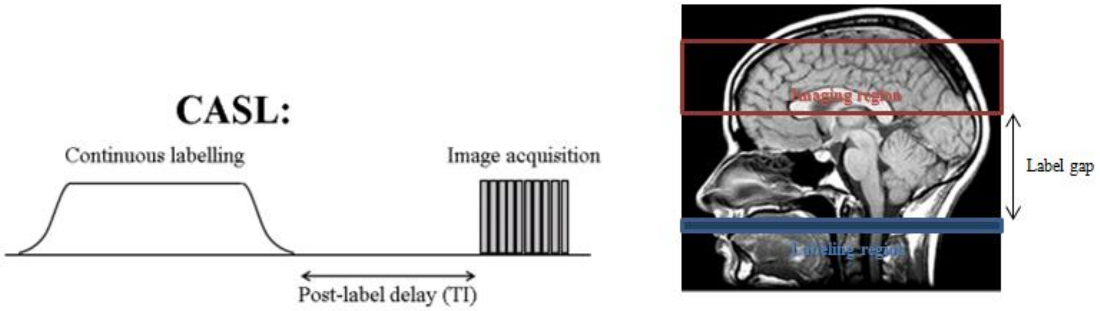

Figure 15 – Diagram depicting CASL: pulse sequence (left) and relative positioning of the imaging and labeling regions (imaging region in red and labeling region in blue, on the right) (adapted from **[18]**).

The most efficient way to achieve continuous inversion is by using a technique called flow-driven adiabatic fast passage (AFP), which inverts the magnetization vector by shifting the resonance frequency of the flowing blood spins through resonance.

The spins that are moving through the labeling plane suffer a gradual change in resonant frequency due to the additional field of the gradient (since it is directly proportional to the magnetic field strength, as previously seen in Eq. 1).

The difference between the resonance frequency of the protons and the transmission frequency changes from positive through negative as the spins move through the inversion plane, and it is zero at its center – there is a “frequency sweep”, making the resonant frequency of the blood water spatially dependent.

Because of this, the effective magnetic field (a combination of $\mathbf{B}_0$, $\mathbf{B}_1$ and the magnetic field resulting from the spin’s precession itself) will rotate from pointing along the direction of $\mathbf{B}_0$ to pointing against it. If this rotation is slow when compared to the precession frequency, the flowing protons will enter a “spin-locked” state, so that their associated magnetization will precess around the effective magnetic field, following it through its rotation and resulting in an inversion of the spins' magnetization as they cross the labeling plane (Fig. 16) [32].

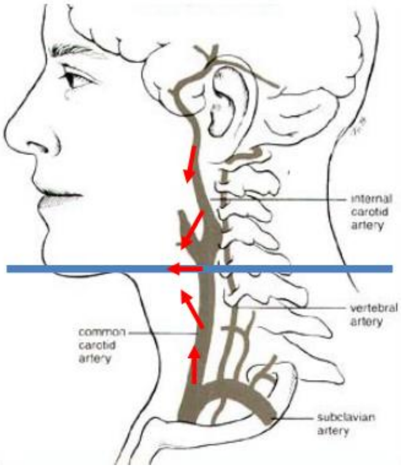

Figure 16 – Spins magnetization variation (red) while flowing through the labeling plane (blue) (adapted from **[33]**).

Even though CASL yields high SNR, the continuous RF labeling may cause significant power deposition in the subject, which means that Specific Absorption Rate (SAR) maximum guidelines may be a limiting issue, particularly when working at high magnetic field strengths. Also, the application of this long inversion pulse in CASL is limited in many commercial scanners.

In addition, this long pulse also induces magnetization transfer (MT) effects, since the application of long off-resonance RF pulses for labeling may cause direct macromolecular saturation in the brain tissue. When saturated, macromolecules exchange their magnetization with the "free" water in the tissue, changing both the apparent T_1 and the M_0 of the blood. The tagged-control subtraction would then indicate not only the perfusion effects, but also the degree of MT, reducing the observed signal and interfering with the CBF quantification.

To overcome this problem, a distal labeling pulse can be applied before acquiring the control image, in order to produce identical MT effects (but symmetrical in frequency), so that the MT effects cancel upon subtraction. However, this only works for single slice acquisitions. To circumvent this, a hardware-based approach can also be used, by placing a small labeling coil on the neck, immediately adjacent to the artery supplying blood to the brain. Since the field of view (FOV) of the labeling coil does not reach the brain, there are no off-resonance effects, also reducing the power deposition in the subject. Multi-slice acquisition with higher SNR is then possible, without subtraction artifacts.

Even though this approach might seem simple to implement, the additional hardware needs to be synchronized with the main MRI scanner's pulse sequence, and it also has the disadvantage of being more uncomfortable for the subject due to the additional neck coil [34, 35].

3.3.2 PASL – Pulsed Arterial Spin Labeling

In PASL, the spins' inversion is achieved by applying a short RF inversion pulse, which will invert the spins in a specific region that contains the arterial supply – the inversion slab (Fig.17).

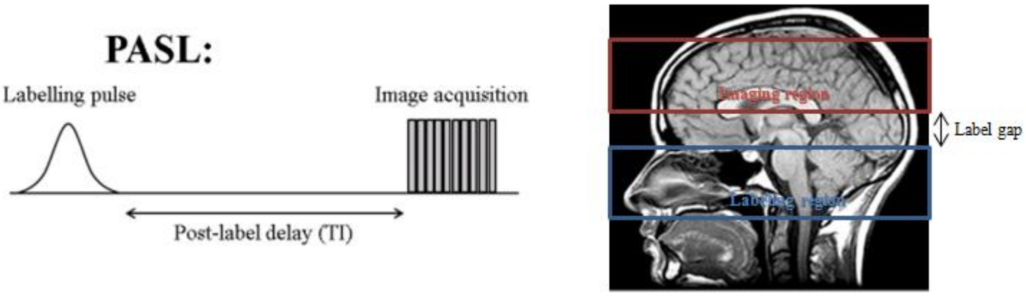

Figure 17 – Diagram depicting PASL: pulse sequence (left) and relative positioning of the imaging and labeling regions (imaging region in red and labeling region in blue, on the right) (adapted from **[18]**).

After the inversion, the inverted blood water in this slab flows into the region of interest, mixing with the non-inverted brain tissue water, after which the image is acquired. The control image is acquired without the slice-selective inversion. The signal intensity difference of the tagged and control images can then be quantified and translated into perfusion images. This process mimics the injection of a tracer bolus, rather than a constant infusion, like previously seen with CASL.

One of the advantages of PASL over CASL is the closer proximity between the inversion labeling slab and the region of interest, minimizing transit time effects (Figs. 15 and 17). Even so, since the imaging and inversion slabs profiles are not perfectly rectangular, a gap between their edges is needed to avoid incomplete subtraction, which would introduce a systematic error in CBF quantification. MT effects are smaller with this technique due to the use of shorter RF pulses, and the SAR is lower as well, but PASL has a reduced sensitivity to flow since the inverted blood water relaxes during the inflow time.

In order to further improve the inversion efficiency in PASL sequences, adiabatic hyperbolic secant (AHS) pulses are usually preferred. These are relatively short adiabatic pulses, insensitive to $\mathbf{B}_1$ field inhomogeneity, which possess a sharp inversion profile [36].

3.3.2.1 PASL sequences

PASL methods like FAIR, PICORE (Proximal Inversion with Control for Off-Resonance Effects) and EPISTAR (Echo Planar Imaging and Signal Targeting with Alternating Radiofrequency) use a single inversion pulse to magnetically label the spins. The difference between them is the location of the labeling plane (Fig. 18) and the choice of the magnetically labeled state of the blood for the control and label images.

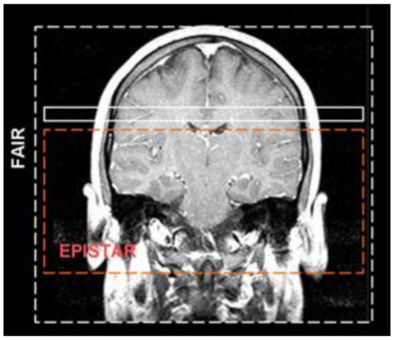

Figure 18 – Pulsed ASL labeling schemes, depicting the labeling planes for EPISTAR (orange line) and FAIR (white line) **[37]**.

EPISTAR is theoretically similar to CASL. After saturation of the imaging slice, a short inversion pulse is applied proximal to the region of interest, followed by a delay (*TI*) to allow the inverted blood to flow into the tissue of interest, in the imaging slice, before acquiring the tagged image using EPI. A control image is also acquired, in which the label is applied symmetrically distal to the imaging slab, thus having the same MT effects.

An EPISTAR variant called PICORE, acquires the control image without a slice-selection gradient.

In FAIR, two IR images are acquired. An inversion pulse is applied over the whole brain (non-selective inversion), labeling all protons, followed by *TI* before acquiring the control image. For the tagged condition, an inversion pulse is applied only to the imaging slices (slice-selective inversion), followed by the same *TI* in order to allow for the blood to flow into the imaging region before acquisition [38].

3.3.3 PCASL – Pseudo-Continuous Arterial Spin Labeling

As previously discussed, PASL has a straightforward implementation and a high and stable tagging efficiency, while CASL has a longer and better defined tagging bolus, and consequently higher SNR. PCASL was developed to take advantage of both PASL and CASL's benefits [39].

The continuous labeling pulse is divided into a rapidly applied train of pulses to achieve the same AFP (as previously described in section 3.3.1). During the control scan, the same pulse train is used but the phase of every other pulse is shifted by 180º, so that these pulses undo the flip of the previous pulse. This way, both the control and tagged images receive the same MT. The flowing blood's magnetization gets inverted before the tagged image is acquired, while remaining un-inverted during the control image acquisition.

The downside is that PCASL is sensitive to magnetic field inhomogeneity at the inversion plane, which may affect the efficiency of the labeling process and is exacerbated at higher magnetic field strengths [40].

3.4 Quantification

The difference between the tagged and control images acquired with ASL is perfusion-weighted, but for absolute quantification an accurate mathematical model of the system is needed, so the measured magnetization difference can be linked to perfusion.

The ideal tissue magnetization difference signal over time is represented in Fig. 19. There are three clearly distinct parts in this curve. First, there is no signal until the labeled protons reach the tissue, during the transit time. Next, when these protons reach the tissue the signal difference increases while there is inflow of labeled water. Finally, the signal decreases due to relaxation and also to the outflow of labeled protons.

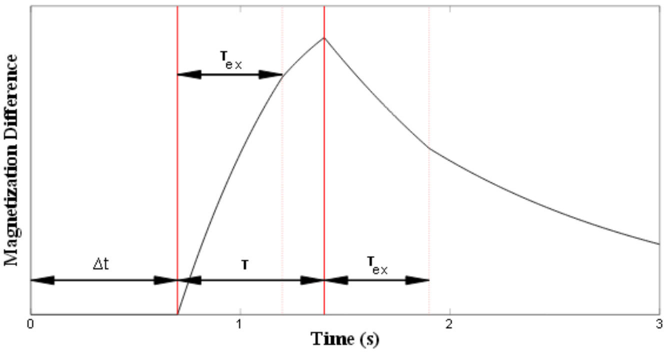

Figure 19 – Magnetization difference as a function of *TI* [41].

Buxton et al. developed a general kinetic model for the difference of magnetization in ASL experiments, where the parameters can be adjusted for CASL or PASL experiments [42].

This model is based on the following functions:

1. $\mathrm{c(t)}$ – delivery function, the normalized arterial concentration of magnetization that arrives at the voxel at time *t*;
2. $\mathrm{r(t, t^{'})}$ – residue function, the fraction of labeled spins that arrived at time *t*’ and are still present at time *t* in the voxel;
3. $\mathrm{m(t, t^{'})}$ – magnetization relaxation function, the fraction of the original M_z tag carried by the water molecules that arrived at *t’* and remains at time *t*.

This model can be described as the following convolution, described in Eq. 7.

$$\Delta M = 2\alpha M_{0\,b} \int_0^t c(t^{'}) \cdot r(t - t^{'}) \cdot m(t - t^{'})\, dt'$$
$$= 2\, M_{0\,b}\, f \,\{\, c(t) * [\, r(t)\, m(t)\,]\,\}$$

Equation 7

In this equation, M_{0b} is the equilibrium magnetization of arterial blood and f is the CBF [42].

By applying single-compartment kinetics, which implies assuming that the exchange between arterial blood and tissue is instantaneous, and that each voxel is a single well mixed compartment, this equation can be rewritten for PASL methods as follows, from Eq. 8 to Eq. 11.

$$\Delta M = \begin{cases} 0 & 0<t<\Delta t \\ 2\, M_{0b} f\, (t - \Delta t)\alpha\, e^{-\frac{t}{T1_b}} q_p(t) & \Delta t<t<\tau+\Delta t\,, \\ 2\, M_{0b} f\, \tau\alpha\, e^{-\frac{t}{T1_b}}\, q_p(t) & \tau+\Delta t<t \end{cases}$$

Equation 8

where

$$q_p(t) = \begin{cases} \frac{e^{kt}(e^{-kt} - e^{-kt})}{k(t - \Delta t)} & \Delta t < t < \tau + \Delta t \\ \frac{e^{kt}(e^{-kt} - e^{-k(\tau + \Delta t)})}{k(\tau)} & \tau + \Delta t < t \end{cases}, \qquad \textbf{Equation 9}$$

$$k = \frac{1}{T_{1b}} - \frac{1}{T_1{'}} \qquad \textbf{Equation 10}$$

and

$$\frac{1}{T_1{'}} = \frac{1}{T_1} + \frac{f}{\lambda}. \qquad \textbf{Equation 11}$$

In these equations, f is CBF in ml of blood/ml of tissue/second (note that in order to change from these units to ml of blood flow/g of tissue/second, its value must be multiplied by the tissue's density), T_{1b} and $T_1{'}$ are the blood's T_1 and the apparent tissue's T_1, respectively, α is the inversion efficiency, λ is the blood-brain partition coefficient, Δt is the arterial transit time and τ is the time width of the label. q_p is a correction factor, related to different relaxation times and venous clearance, and typically has a value close to 1.

ΔM is proportional to f, but it does not provide enough data for a quantitative perfusion map, since it lacks information about Δt and τ. Both M_{0b} and T_{1b} are spatially invariant constants, that can either be estimated from measurements or based on literature values.

In order to determine the labeling efficiency α in PASL, it is necessary to do measurements at different inversion times both in phantoms and *in vivo*. This value can generally be very close to 100%. M_{0b} is obtained from a separate scan, before any acquisitions or inversions [42].

Applying Equations 8 to 11 to PASL, the following expressions are obtained, which were used in this project, presented on Eq. 12 and Eq. 13 [4]:

$$\Delta M(t) = \frac{f}{\lambda} 2\alpha M_{0b} \; \frac{e^{\frac{-t}{T1'}}}{\frac{1}{T_a}} \left(e^{\frac{t}{T_a}} - e^{\frac{\Delta t}{T_a}} \right), \qquad \textbf{Equation 12}$$

where

$$\frac{1}{T_a} = \frac{1}{T_1{'}} - \frac{1}{T_{1b}}. \qquad \textbf{Equation 13}$$

3.5 fMRI – ASL versus BOLD

CBF changes can be used as a biomarker for regional brain function changes.

As previously stated, the standard approach to fMRI is BOLD, but ASL has proven to have some advantages over BOLD. ASL can provide absolute quantification of perfusion, which allows for more accurate comparisons, both inter and intra-subject (since BOLD is more sensitive to non-physiological factors, these variations are lower in perfusion MRI) [18].

Additionally, BOLD is more weighted towards draining veins, so activation changes may be detected slightly downstream from the specific activated area, which has a higher metabolic rate in the brain tissue. There is evidence that suggests that perfusion changes have superior spatial and temporal specificity to neural activation than BOLD during a typical fMRI paradigm, making CBF changes more localized to the brain parenchyma than the BOLD effect. Perfusion fMRI based on ASL methods may then offer more accurate measurements of spatial localization and magnitude of neural activation [35, 43].

As previously mentioned, the BOLD signal is a complex function, dependent on CBF, $CMRO_{2,}$ CBV and magnetic field strength. Changes in any of these parameters caused by disease, age or other factors can complicate the analysis of BOLD's signal variations.

Perfusion measurements are also insensitive to low-frequency fluctuations often observed in BOLD studies. In regions of high static susceptibility like the orbital-frontal cortex, there is loss of signal when using BOLD. ASL can use imaging sequences less sensitive to signal loss caused by these magnetic susceptibility effects.

However, the SNR of ASL is considerably lower and ASL requires longer scan time when compared to BOLD, since it requires many averages to overcome the low SNR. Additionally, event-related fMRI is nigh impossible with ASL. It is also important to consider that BOLD is much simpler to use and is much more widespread, regardless of its considerable disadvantages listed herein.

Even so, ASL can complement the information given by BOLD, by providing quantitative measurements of both baseline and changes in CBF, helping in the analysis of BOLD signal changes. When combined with BOLD, both methods can measure the changes in oxygen use that accompanies changes in behavior [8].

ASL allows for a different functional approach by correlating rest perfusion with cognitive performance. Resting-state BOLD fMRI also allows for a qualitative analysis in studies of this kind. This can remove the need for task-related paradigms inside the MRI scanner, in which the participants may perform poorly, benefitting studies focused on particular patient groups like the elderly [18].

Regarding both techniques, it is also important to state that although there is a recognized coupling of CBF and metabolism in the working brain, the mechanisms behind this coupling are not yet fully understood. It is normally assumed that an increase in CBF is required to supply nutrients and oxygen for neural metabolism, but studies of brain energy metabolism have yet to conclusively support this idea. Alternatively, the increase of CBF may be required to remove toxic waste products of metabolism [18]. These topics are summarized in Table 2.

Table 2 – Summary of the comparison between ASL and BOLD when measuring neural activation (adapted from **[8]**).

Advantages of ASL versus BOLD	Disadvantages of ASL versus BOLD
Absolute quantification of a physiological parameter, with less intra and inter-subject variability than BOLD.	ASL response SNR is typically half of the BOLD response SNR.
Processing of ASL data by using difference minimizes the effects of low frequency drifts and makes this method more useful for experiments with longer stimulus duration.	Temporal resolution of ASL is lower than BOLD’s, since it needs to acquire both tag and control images, and also wait for the blood to reach the imaging region.
ASL can be used in conjunction with imaging methods like SE-readouts that reduce signal loss due to magnetic susceptibility variations.	The maximum number of slices that can be acquired with ASL is less that with BOLD, because of the need to acquire data before the labeled signal has fully relaxed.
The ASL perfusion signal is well localized to the capillary beds.	ASL is not as simple to acquire and process as BOLD.

Chapter 4
Methodology

This chapter includes a description of the methods used throughout the project. A general overview and biological background of the procedures used is presented, as well as specifics of the different experimental steps.

4.1 Brief overview

The different experimental stages of this project were conducted in an evolutionary process of optimization. The first step consisted on further optimizing the FAIRPRESS sequence [4] for perfusion measurements in WM.

Secondly, the optimized sequence was used to measure perfusion during functional activation, both in grey and white matter. The activation stimulus used was a rotating circular checkerboard with changing colors. The first acquisitions were done once for each voxel position (single acquisition), in the GM of the visual cortex (VC) and in the *corpus callosum* (CC). For one subject, data was also acquired once in the WM of the VC. Afterwards, the measurements in WM were performed twice for the same position (double acquisition), for both the CC and WM of the VC, while using shorter stimuli blocks and fewer repetitions. For all these measurements, the T_2* was also measured and analyzed.

Afterwards, different pulse sequences were tested in order to find out which one yielded the best results for perfusion measurements in WM: the previously optimized FAIRPRESS, FAIRPRESS with background suppression (BS) and PCASL. After analyzing the results, it was concluded that FAIRPRESS with BS was the best method.

This sequence was then used in conjunction with an adaptation of the Poffenberger task (previously reported to elicit activation in the anterior part of the CC) [44], to measure both perfusion and T_2* variations during activation in the CC. These measurements were performed three times for the same voxel position (triple acquisition), using the same size in blocks and repetitions as the double acquisition measurements with the purely visual stimulus in the CC. One measurement was also performed on the GM of the VC.

Finally, whereas the previous steps were conducted in a 3T scanner, additional experiments were conducted in the ultra-high magnetic field of 9.4T. Considering the SAR limitations when working with such a strong magnetic field, the sequence used was FAIRPRESS without BS nor pre-saturation, and with only two saturation bands (above and below the voxel of interest). The adapted Poffenberger task was again used for stimulation, and measurements were performed both in the CC and in the GM. This overview is summarized in the flow chart displayed in Fig. 20.

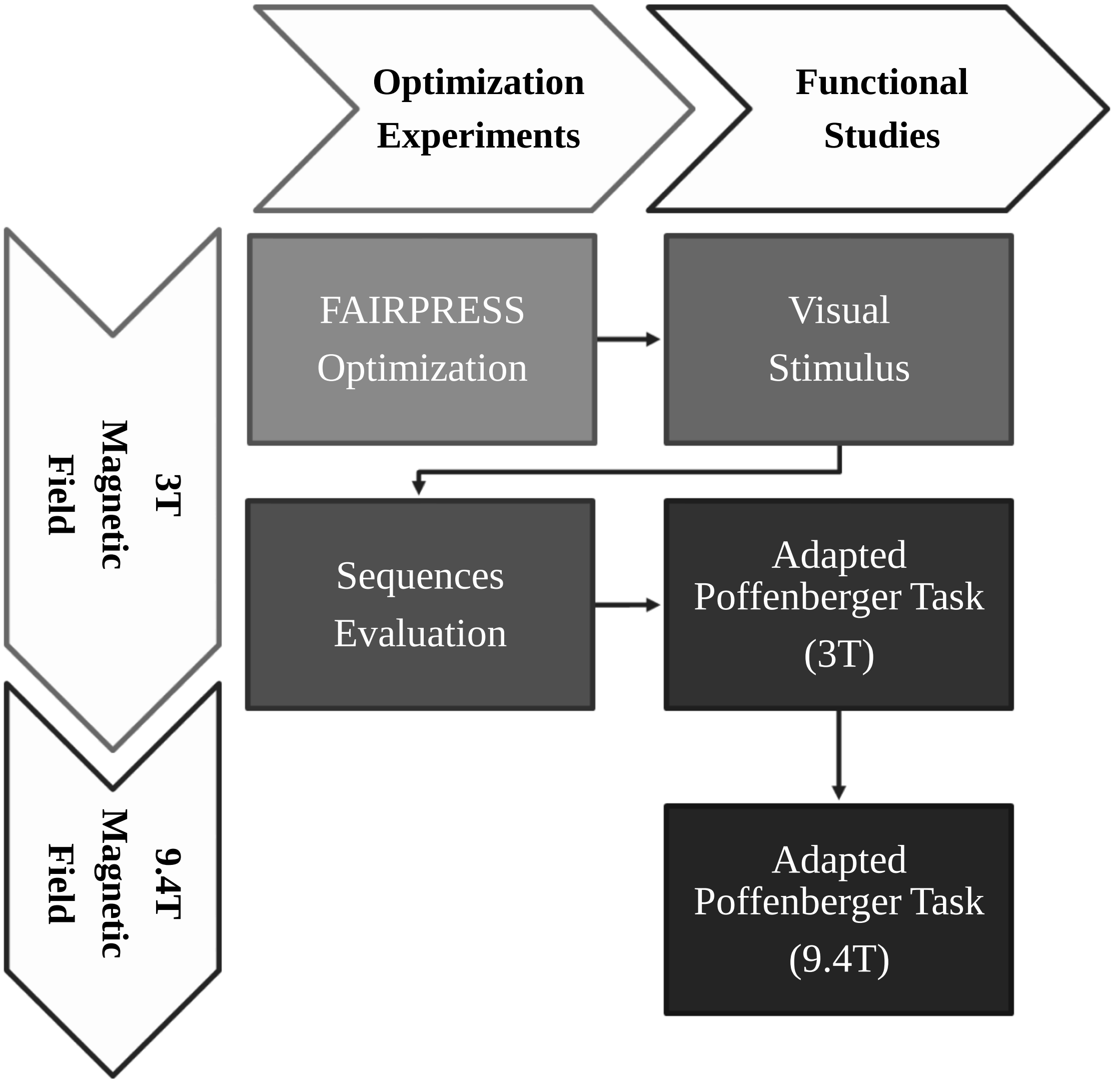
Optimization Experiments
Functional Studies
3T Magnetic Field
9.4T Magnetic Field
FAIRPRESS Optimization
Visual Stimulus
Sequences Evaluation
Adapted Poffenberger Task (3T)
Adapted Poffenberger Task (9.4T)

Figure 20 – Flow chart describing the chronological evolution and optimization of the project.

4.2 Biological background

4.2.1 Brain

The brain is a complex and extensive organ. It consists of billions of cells and is composed mainly of two different types of tissue: white matter and grey matter.

The GM is composed of neuronal cell bodies, glial cells (specifically oligodendrocytes and astroglya) and the neuropil (composed by dendrites, and myelinated and unmyelinated axons). It is involved in multiple tasks, such as sensory perception, memory, seeing, hearing and muscle control [45].

The WM is composed by myelinated axons and glial cells, connecting the neurons through fiber pathways. Myelin is a fatty protein responsible for insulation and speed increase of transmission, giving WM its white color. WM modulates the distribution of action potentials, coordinating communication between different brain regions [46].

4.2.2 *Corpus Callosum*

The CC is a WM fiber bundle that connects the two brain hemispheres, facilitating the transmission of visual, sensory and cognitive information between them. It is the largest WM structure in the brain, and is one of the few white matter tracts that can be discretely identified by conventional MRI.

It can be divided in 4 regions, represented in Fig. 21. The *rostrum*, the *genu* (formed mostly by interfrontal fibers), the *isthmus* (main portion of the CC, allowing for interparietal and intertemporal communication) and the *splenium* (allows for interhemispheric communication between the parietal, temporal, and occipital lobes) [47].

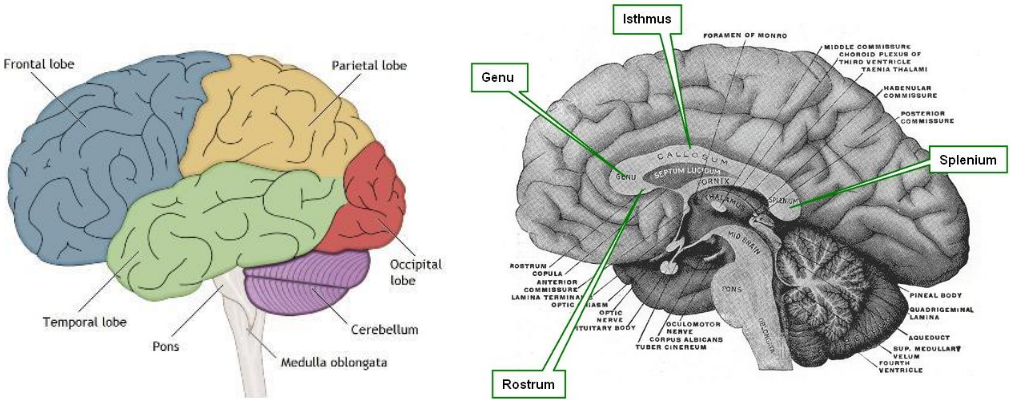
Frontal lobe
Parietal lobe
Occipital lobe
Temporal lobe
Cerebellum
Pons
Medulla oblongata
Isthmus
Genu
Splenium
Rostrum
FORAMEN OF MONRO
MIDDLE COMMISSURE
CHOROID PLEXUS OF THIRD VENTRICLE
TAENIA THALAMI
HABENULAR COMMISSURE
POSTERIOR COMMISSURE
CALLOSUM
GENU
SEPTUM LUCIDUM
FORNIX
THALAMUS
SPLENIUM
MID BRAIN
PONS
OBLONGATA
ROSTRUM
COPULA
ANTERIOR COMMISSURE
LAMINA TERMINALIS
OPTIC CHIASM
OPTIC NERVE
PITUITARY BODY
OCULOMOTOR NERVE
CORPUS ALBICANS
TUBER CINEREUM
PINEAL BODY
QUADRIGEMINAL LAMINA
AQUEDUCT
SUP. MEDULLARY VELUM
FOURTH VENTRICLE

Figure 21 – **Left**: Lateral view of the brain's division into lobes **[48]**. **Right**: Sagittal view of the brain, centered on the *corpus callosum*, its regions highlighted **[47]**.

Two studies have established a topographical distribution on the CC of the fiber tracts connecting to the cortex (Fig. 22) [49, 50]. The division of the CC performed by Hofer is generally more accepted, since it was done in human subjects, while the Witelson study was based on primate data).

Based on Hofer's CC topography, the CC is divided in five parts. Axons in the *genu* of the CC connect the prefrontal cortex of each brain hemisphere (Region I, Fig. 23). The anterior midbody of the CC connects the premotor and supplementary motor cortical areas (Region II, Fig. 23), and the posterior half of the CC is divided in three, where fibers connect the primary motor, sensory and visual cortical areas (Regions III, IV and V, respectively, in Fig. 23).

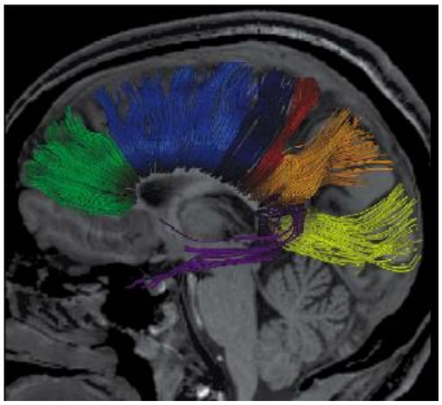

Figure 22 – Sagittal view of a 3D reconstruction of all callosal fibers comprising bundles projecting into the prefrontal lobe (green), premotor and supplementary motor areas (light blue), primary motor cortex (dark blue), primary sensory cortex (red), parietal lobe (orange), occipital lobe (yellow), and temporal lobe (violet) **[49]**.

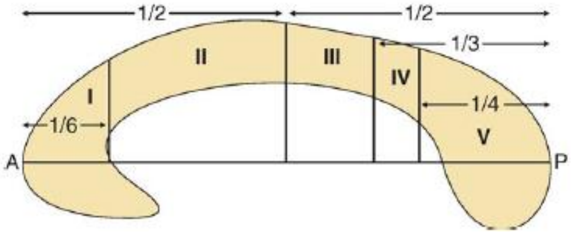

Figure 23 – Hofer's CC topography. Region I: prefrontal; region II: premotor and supplementary motor; region III: motor; region IV: sensory; region V: parietal, temporal, and occipital. A: anterior; P: posterior **[49]**.

4.2.3 Visuo-Motor Interhemispheric Transfer

The human VC is located in the occipital lobes of both brain hemispheres (Fig. 21, left). The primary VC is responsible for transmitting visual information from the retina to the other cortical regions of the VC. The left hemisphere visual cortex receives information from the right visual field, and the right hemisphere VC from the left visual field, by means of the optic chiasm.

The following described tasks were designed in order to elicit interhemispheric transfer:

- **Poffenberger paradigm:**

  During this task, light flashes are presented rapidly to the left or right visual hemifield, and the subject is asked to respond with either the contralateral (crossed) or ipsilateral (uncrossed) hand. This has been proven to elicit white matter activation in the anterior part of the *corpus callosum*, being the most well-established case of WM fMRI activation [6, 51];

- **Sperry paradigm:**

  Word and face stimuli associated with the left and right hemisphere, are presented rapidly to the right or left visual hemifield, respectively. In this case, the crossed condition is when the stimulus is presented to its contralateral hemisphere (i.e. presenting face stimuli to the left hemisphere via the right visual hemifield). This task has been shown to elicit activation in the CC, in its posterior portion [52].

4.3 Sequences

The three different sequences used were developed having WM particularities in mind, such as its intrinsically low perfusion and its long and inhomogeneous transit delay. They were tested to assess which yielded the best results for measuring WM's perfusion.

4.3.1 FAIRPRESS

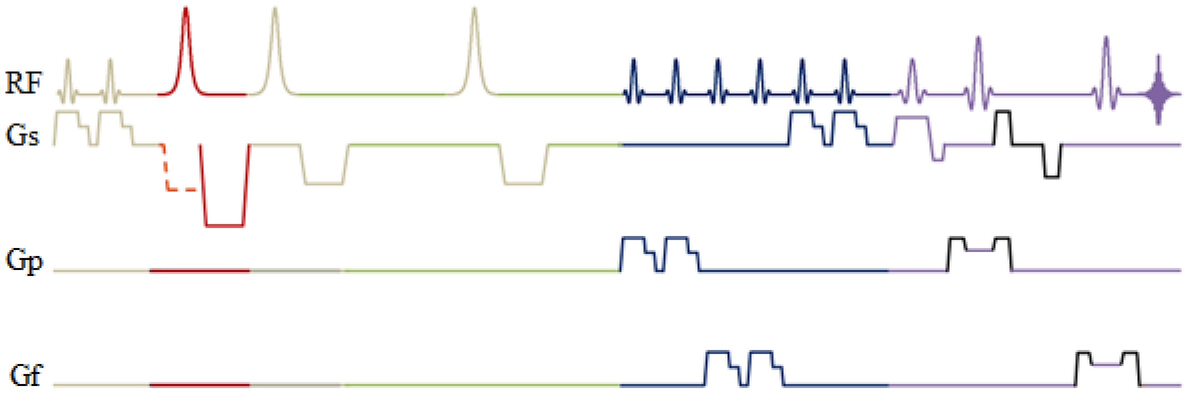

Figure 24 – FAIRPRESS sequence. Background suppression (green), FAIR's perfusion encoding (red), slice selection only in tag scans (orange), outer volumes suppression (blue), PRESS volume selection (purple) and strong bipolar gradients (black).

In Fig. 24, the BS pulses and gradients are represented in green; they are omitted in experiments without BS. First, the perfusion is encoded using FAIR (red), with slice selection only in the tag scans (orange dashed line). As shown above, FAIR requires the subtraction between the signal acquired with a global inversion pulse (control) and the signal acquired with a local inversion pulse (tag). For inversion, a highly selective adiabatic inversion pulse was used.

The next 6 pulses (blue), with two gradients along each direction, correspond to the saturation slices in all directions around the voxel of interest, for outer volume suppression (OVS) to avoid partial volume effects. The subsequent three pulses are from the PRESS volume selection (purple), accompanied by strong bipolar gradients (black) to dephase the magnetization from the flowing blood in order to reduce the contribution from larger vessels.

The acquisition is done alternating between tag and control. The first scan is done without the inversion pulse, in order to obtain M_0 – the reference magnetization, which is needed for quantification.

4.3.2 FAIRPRESS with background suppression

BS was introduced in order to cancel the signal from static tissue by applying two saturation pulses before the tag and two inversion pulses during *TI* (green, Fig. 24). The image is then acquired when the M_z of the tissue is zero. Two spin populations with different T_1s can both be nullified by using two inversion pulses with adequate sequence timing. Background suppression has been shown to result in a significant increase in the SNR of perfusion measurements with ASL [53].

The rest of the sequence used was the same as above for FAIRPRESS without background suppression.

4.3.3 PCASLPRESS

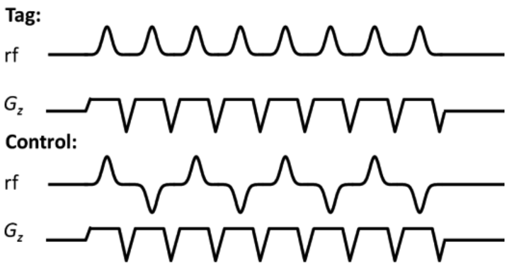

Figure 25 – PCASLPRESS's labeling scheme (balanced PCASL).

As previously introduced in section 3.3.1, in CASL, the blood passing through a narrow slice in the neck is continuously labeled for approximately 2s, using a low power RF pulse, resulting in a steady state of flow driven adiabatic inversion. This mimics the injection of a constant infusion of a tracer and yields high SNR, but also results in significant RF power deposition in the subject. This, in conjunction with the previously mentioned implementation issues of this technique, gave way to the development and great interest in PCASL (section 3.3.3 of this thesis), as an alternative to overcome these issues. PCASL achieves the same flow driven adiabatic inversion, but instead of using a continuous labeling pulse, it is split up in multiple shorter pulses (Fig. 25).

Therefore, this labeling was also tested in order to see if the resulting longer and better defined tagging bolus would generate a higher SNR in WM perfusion measurements than FAIR. The rest of the sequence used, besides the labeling scheme depicted in Fig. 25 (used instead of FAIR) was the same as previously seen for FAIRPRESS without BS.

4.4 Participants

A total of 26 healthy volunteers, with ages between 22 and 46 were scanned, after providing written informed consent. The participants received monetary compensation for their participation in the experiment.

Of these, 7 participated in the sequence optimization experiment, 9 in the visual stimulus experiments, 8 in the adapted Poffenberger task experiments in the 3T MRI scanner and 2 others in the adapted Poffenberger task experiment at the 9.4T magnetic field.

4.5 Experimental design

4.5.1 Sequence Optimization

The data regarding both FAIPRESS parameter's optimization and the three different sequences evaluation was acquired during rest, in order to assess which of the tested parameters and sequences yielded the best perfusion measurement results.

4.5.2 Functional Studies

A fixation cross was displayed in the center of the screen for the duration of the activation experiments, and the subjects were asked to maintain central fixation throughout. The stimuli were displayed using back-projection to a screen placed inside the bore, viewed through a mirror mounted on the head coil. The rest condition, for all the stimulus experiments, consisted of a grey screen with the white fixation cross displayed in the middle of the visual field.

A summary of the experimental designs used for the activation experiments is depicted in Table 3. All stimuli were presented in a block design with the same number of alternating rest and stimuli blocks (half of the blocks presented in Table 3 for stimulus and half for rest). Note that the number of blocks depicted is per acquisition, meaning that for the double and triple acquisitions, the total number of blocks should be multiplied by two and three, respectively. Also note that the duration shown is for single blocks.

Table 3 – Summarized experimental design for the activation experiments.

Experiment	Sequence	Acquisition	Tissue	Design	
				Blocks	**Duration (s)**
Visual Stimulus	T_2*-EPI	Single	GM (VC)	12	10.00
	FAIRPRESS	Single	GM (VC)	14	68.16
			WM (CC and VC)		
		Single	GM (VC)	20	34.08
		Double	WM (CC and VC)	12	51.12
Adapted Poffenberger Task (3T)	FAIRPRESS with BS	Single	GM (VC)	20	34.08
		Triple	WM (CC)	12	51.12
Adapted Poffenberger Task (9.4T)	FAIRPRESS (adjusted)	Single	GM (VC)	12	51.12
		Double	WM (CC)		

4.5.2.1 Visual stimulus

The participants were asked to simply look at the visual stimulus throughout the experiment. It consisted of a color changing rotating checkerboard, presented to the central visual field (Fig. 26). Its presentation was done using Cogent [54], running in MATLAB (The Mathworks Inc., Natick, MA).

A T_2*-weighted EPI acquisition was first performed to locate activated regions for voxel positioning (Fig. 33, on section 4.6.2 of this dissertation).

FAIRPRESS experiments were performed initially as single acquisition measurements, in the GM of the VC and in the WM of the CC, for 5 subjects, using long blocks for both. In one subject, a measurement in the WM of the VC was also performed, using the same block design as in the CC. Secondly, double acquisition measurements using more blocks with shorter durations were performed for WM, both in the CC and in the VC, for 4 subjects. For these subjects, a single acquisition in the GM used more blocks with shorter length (Table 3).

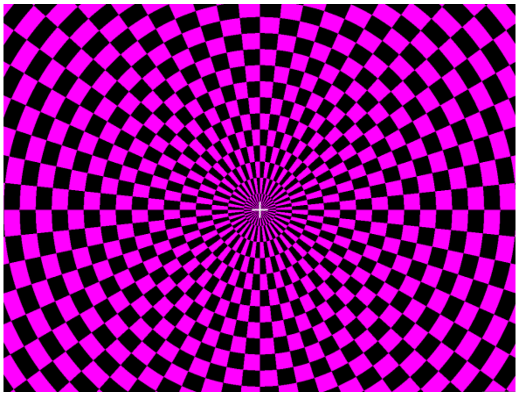

Figure 26 – Still frame of the visual stimulus used.

4.5.2.2 Adapted Poffenberger task

The participants were asked to perform a variation of the Poffenberger task. The stimulus consisted of a color changing rotating checkerboard, presented to either the left or right visual hemifield in randomized order (Fig. 27). The subjects were given two button boxes, one for each hand, and were asked to repeatedly perform a simple button-pressing sequence, during the presentation of the stimulus. The response hand was crossed for all trials (i.e. when the checkerboard was presented to the left visual hemifield, the subject replied with his right hand, and vice-versa), since this had been shown previously to elicit more activation than the ipsilateral response [44]. The stimuli were presented rapidly (100ms per change) to avoid saccades. Presentation was done using MATLAB and the Psychophysics Toolbox extension [55].

The FAIRPRESS experiments with BS at 3T where the aforementioned task was performed used triple acquisition in the CC in a total of 8 subjects. The block design used was the same as for the double acquisition experiments with the visual stimulus presented in last section. For one of these subjects, a single acquisition was performed in the GM of the VC, using a similar block design but more and shorter blocks (Table 3).

The adjusted FAIRPRESS experiments at 9.4T consisted in a single acquisition for GM in one subject and double acquisition in the CC for two subjects, both using the same block design as the CC measurements performed at the 3T scanner (Table 3).

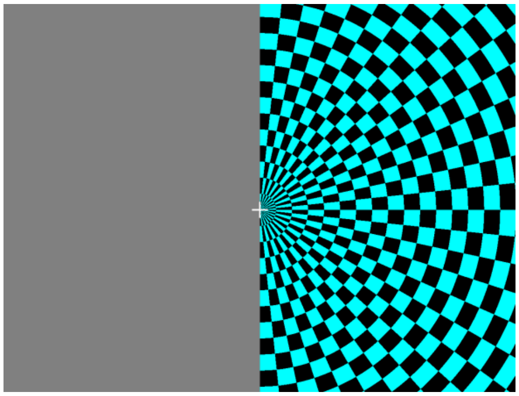

Figure 27 – Still frame of the visual stimulus used for the adapted Poffenberger task.

4.6 Data Acquisition

All experiments at a magnetic field of 3T – FAIRPRESS optimization and the different sequences evaluation, as well as the functional activation experiments – were performed on a Siemens Magnetom Prisma (Siemens Medical Solutions, Erlangen, Germany) scanner, using a 20-channel bird-cage coil for reception. The body coil was used for RF transmission. To restrict motion, the subjects' head was stabilized with foamed material inside the head coil.

For every subject, localizer images were acquired, followed by an anatomical image using the MPRAGE sequence, which were used later for voxel placement in the areas of interest, as well as for correctly positioning the labeling slice in PCASLPRESS (Fig. 28). The MPRAGE was acquired with TR = 1750ms, TE = 2.84ms, TI = 1100ms and TA = 5min17s, flip angle = 9º, matrix size = 180x192, FOV = 256x240mm, and a slice thickness of 1.30mm.

For perfusion quantification, an 8x8x5mm^3 voxel was used. It was carefully positioned to avoid contributions from surrounding tissues.

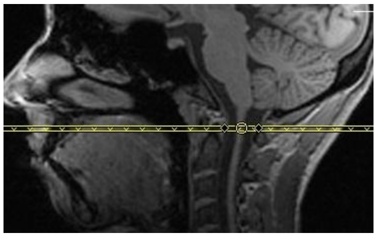

Figure 28 – PCASLPRESS's labeling plane, placed on the MPRAGE. Its positioning was based on PCASL's optimization studies found in the literature **[56]**.

4.6.1 Sequence Optimization

The three sequences were tested by performing perfusion measurements in both white and grey matter during rest. The WM region chosen for these tests was the CC.

For verification of the perfusion sensitivity, two measurements that were expected to yield no perfusion signal were performed, either by positioning the voxel in the ventricle (for three subjects) or by increasing the thickness of the FAIRPRESS label slice until no labeled blood can reach the voxel site within the inversion delay. The latter can be achieved by increasing the parameter Inversion Slice Factor (ISF) to 99.9. In PCASLPRESS, this can be reached by positioning the labeling plane distally from the voxel of interest.

For FAIRPRESS without BS, the parameters used were: bandwidth = 1000Hz, TR = 2130ms, TE = 29ms, TI = 1200ms, flip angle = 90º, ISF = 3, voxel size = 8x8x5mm and no pre-saturation.

FAIRPRESS with BS was the same, except for the presence of pre-saturation pulses. The used tissue T_1 for WM was 919ms and for GM 1711ms, which had been previously measured using this sequence [4].

For PCASLPRESS, parameters were: bandwidth = 1000Hz, TR = 3670ms, TE = 30ms, tag delay = 1600ms, tag duration = 1500ms, tag pulse angle = 28º and voxel size = 8x8x5mm.

The voxel was positioning in the CC is presented in Fig. 29.

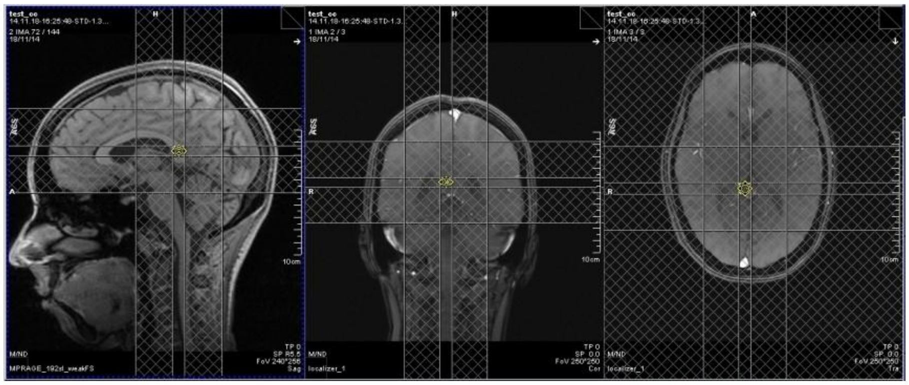

Figure 29 – Voxel positioning on the CC, sagittal (MPRAGE), coronal and transverse views (localizer).

To facilitate positioning the voxel in the region of interest in GM or in the ventricles, a T_2-weighted Turbo Spin Echo (TSE) image with 7 slices was acquired. The parameters thereof were: slice thickness = 2.7mm and a distance factor = 10%, TR = 5180ms, TE = 11ms, TI = 900ms, TA = 2min1s matrix size = 384x512, FOV = 220x220mm and turbo factor = 35.

Voxel placement when measuring in the GM of the VC is depicted in Fig. 30 and in the ventricle in Fig. 31.

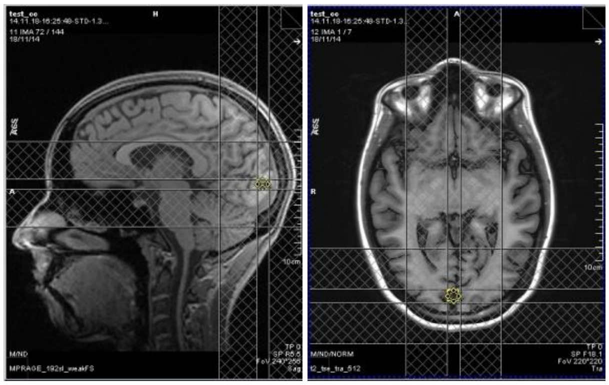
test_oe
14.11.18-16:25:48-STD-1.3...
11 IMA 72 / 144
18/11/14
H
A
10cm
M/ND
MPRAGE_192sl_weakFS
TP 0
SP R5.5
FoV 240*256
Sag
test_oe
14.11.18-16:25:48-STD-1.3...
12 IMA 1 / 7
18/11/14
A
R
10cm
M/ND/NORM
t2_tse_tra_512
TP 0
SP F18.1
FoV 220*220
Tra

Figure 30 – Voxel positioning in grey matter, sagittal (MPRAGE), and transverse views (TSE).

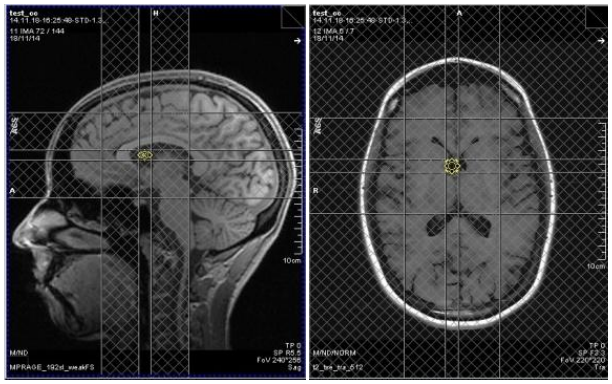
test_oe
11 IMA 72 / 144
H
A
10cm
M/ND
MPRAGE_192sl_weakFS
TP 0
SP R5.5
FoV 240*256
Sag
test_oe
A
R
10cm
M/ND/NORM
t2_tse_tra_512
TP 0
SP F2.3
FoV 220*220
Tra

Figure 31 – Voxel positioning on the ventricles, sagittal (MPRAGE), and transverse views (TSE).

Summarized information about the sequence optimization experiments, such as acquisition times, total measurements performed (both tag and control) and perfusion measurements used for analysis, in which the first two tag/control pairs were discarded, is presented in Table 4.

Table 4 – Summarized experimental design for the activation experiments.

Experiment	Tissue	Sequence	Measurements	*TA*	Perfusion measurements
Sequence Optimization	CC	FAIRPRESS	200	7min 6s	98
		FAIRPRESS BS			
		PCASLPRESS	120	7min 20s	58
	GM, ventricle and no perfusion labeling	FAIRPRESS	120	4min 16s	58
		FAIRPRESS BS			
		PCASLPRESS	70	4min 17s	33

4.6.2 Functional Studies

Summarized information about the activation experiments, such as acquisition times, total measurements performed (both tag and control) and perfusion measurements used for analysis, in which the first four tag/control pairs were discarded, is presented in Table 5. Note that the number of measurements and acquisition times depicted is per acquisition, meaning that for the double and triple acquisitions, they should be multiplied by two and three, respectively.

Table 5 – Summarized experimental design for the activation experiments.

Experiment	Acquisition	Tissue	Sequence	Measurements	*TA*	Perfusion measurements
Visual stimulus	Single	GM (VC)	FAIRPRESS	456	16min 11s	224
		WM (CC and VC)				
	Double	GM (VC)		328	11min 39s	160
		WM (CC and VC)		296	10min 30s	144
Adapted Poffenberger (3T)	Single	GM (VC)	FAIRPRESS BS	328	11min 39s	160
	Triple	WM (CC)		296	10min 30s	144
Adapted Poffenberger (9.4T)	Single	GM (VC)	Adjusted FAIRPRESS	296	10min 30s	144
	Double	WM (CC)				

4.6.2.1 Visual stimulus

In the first stage of the project, perfusion was measured during the presentation of a visual stimulus, using the original FAIRPRESS sequence without BS.

Perfusion measurements were performed in the CC, in the area associated with the intercommunication of visual information between hemispheres, associated with the occipital lobe, as seen in Fig. 22 (in yellow) and Fig. 23 (region V).

Additional experiments were performed with the voxel positioned in the VC, located in the occipital lobe, both in the grey and white matter. In acquiring these images, extra care was taken when positioning the voxel so as to minimize contributions of other tissues.

To facilitate accurate voxel positioning in the activated region of the VC, a functional BOLD experiment using a T_2*-weighted-EPI sequence was performed. The activation maps obtained in this experiment served to localize regions with strong BOLD signal, where the perfusion measurements were then located (Fig. 33). The acquisition of 7 slices had the following parameters: slice thickness = 2,7mm and distance factor = 10%, TR = 1000ms, TE = 30ms, TA = 2min 7s flip angle = 60º, matrix size = 94x94, FOV = 192x192mm and 120 measurements. The FAIRPRESS parameters were the same as previously used for FAIRPRESS without BS, on section 4.6.1 of this thesis, except the TI was 1500ms for all the experiments.

In all experiments, an additional TSE image with good contrast between white and grey matter was acquired for accurate positioning of the voxel in both tissues, using the same parameters as specified in section 4.6.1 and the same slice positions as in the BOLD images. These images were used for the purpose of locating voxels in or close to activated GM areas as well as to detect subject motion between scans (Fig. 32).

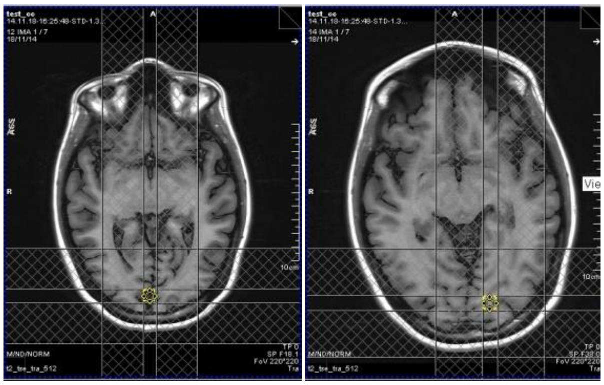

Figure 32 – Transversal view of the voxel positioned on grey (left) and white (right) matter in the visual cortex (TSE).

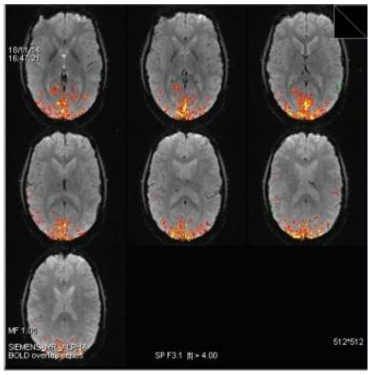

Figure 33 – T_2*-weighted EPI results, acquired during the visual stimulus presentation. The significantly activated areas are superimposed on anatomical images.

4.6.2.2 Adapted Poffenberger task (3T)

After determining that FAIRPRESS with BS yielded the best results, it was used for acquiring the stimulation data for the adapted Poffenberger task. For one subject, the voxel was positioned in the GM of the VC and the signal was acquired once. All the other measurements were acquired three times for the same voxel, in the anterior part of the CC. The voxel position was selected based on previous studies report BOLD activation in the CC and on Hofer's CC topography (Fig. 23) [6, 51]. The *TI* used was 1500ms, and the rest of the parameters were the same as previously used for FAIRPRESS with BS in section 4.6.1 of this dissertation.

To be sure that the subject had not moved between acquisitions, TSE images were acquired between the different repetitions of the experiment, using the same parameters as described in section 4.6.1 of this thesis.

4.6.2.3 Adapted Poffenberger Task (9.4T)

The functional activation experiments at higher field strength were performed on a Siemens Magnetom 9.4T (Siemens Medical Solutions, Erlangen, Germany) scanner with a magnetic field strength of 9.4T, using a 31-channel receive array in combination with a 16 channel transmit coil [57]. Foamed padding was placed inside the head coil to keep the subjects' head stabilized.

Due to the severe SAR limitations at a magnetic field as strong as 9.4T, the sequence parameters had to be adjusted. Therefore, the FAIRPRESS sequence with no BS was used, and instead of 6 saturation bands around the voxel of interest only two were applied, proximally and distally, to avoid vascular contributions. The parameters used were: bandwidth = 2000Hz, *TR* =

2130ms, *TE* = 29ms, *TI* = 1500ms, flip angle = 60º, ISF = 2.5, voxel size = 8x8x5mm^3 and no pre-saturation. The voxel was carefully positioned to avoid contributions from the surrounding tissue.

For measurements in the CC, the voxel was again placed in the region purportedly activated by the Poffenberger task, in its anterior portion (Fig. 34).

A FLASH (Fast Low Angle Shot) 2D sequence was used as anatomical scan, to facilitate the positioning of the voxel in the target areas. The parameters used for this scan were: 18 slices, thickness = 1mm, image matrix size = 464 x 512, FOV = 192 x 174 mm^2, *TR* = 800ms and *TE* = 12ms. Between scans, to check if the subject had moved, another FLASH 2D was used, though with only 6 slices, image matrix = 348x384 and *TR* = 100ms.

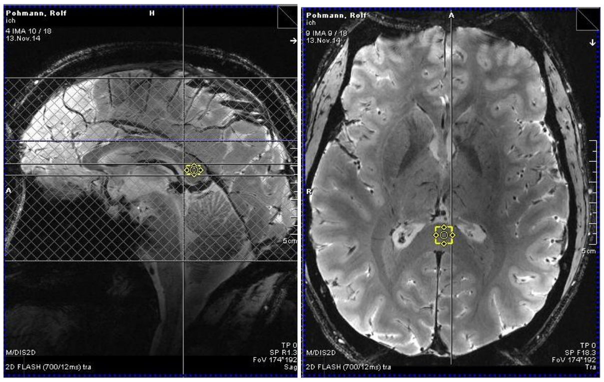
Pohmann, Rolf
ich
4 IMA 10 / 18
13.Nov.14
H
A
5cm
M/DIS2D
2D FLASH (700/12ms) tra
TP 0
SP R1.3
FoV 174*192
Sag
Pohmann, Rolf
ich
9 IMA 9 / 18
13.Nov.14
A
R
5cm
M/DIS2D
2D FLASH (700/12ms) tra
TP 0
SP F18.3
FoV 174*192
Tra

Figure 34 – Voxel positioning in the CC. Sagittal (left) and transversal (right) views.

4.7 Postprocessing

The postprocessing was performed on the raw data, using home-written routines in MATLAB. In general, for every measurement, the single FIDs from each individual coil channel were exponentially filtered for noise reduction and better integration. They were also 4-fold zero filled prior to the FT, in order to increase frequency resolution in the resulting spectra, allowing for better integration over the peaks. The data was then Fourier transformed and combined by adding the root of the sum of squares of the individual signals from the different coils, thus reconstructing the data.

The central 200 points of the water line peak were used for analysis (Fig. 35).

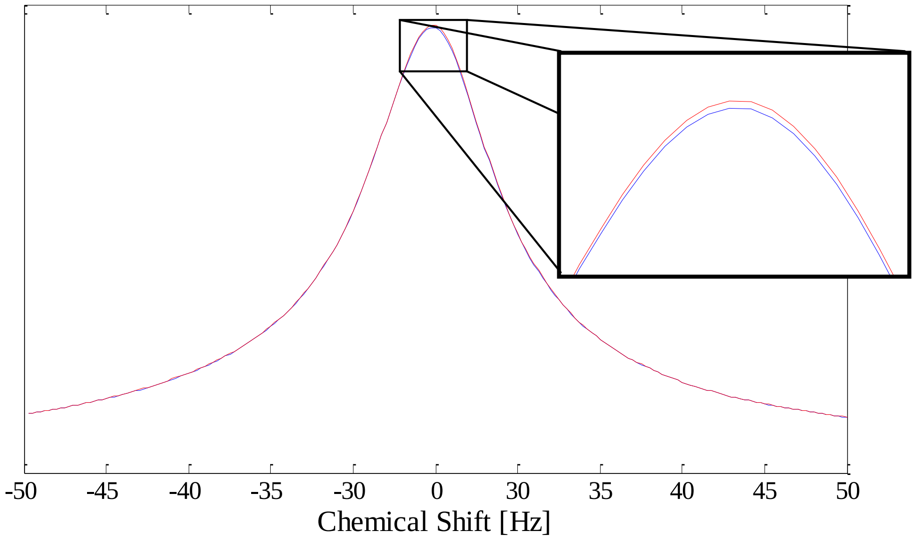

Figure 35 – Central points of the water spectra from the tagged (blue) and control (red) scans from a WM voxel. The difference between them is very small for WM, and slightly larger for GM.

M_0 was taken from the first scan of each series, acquired without any preceding pulses.

For determining ΔM, the 4 first tag/control pairs were discarded in the stimulus experiments, as were the first two in the sequence optimization experiments.

The T_1s considered for the quantification parameters for measurements at 3T were: $T_{1\mathrm{WM}}$ = 919ms, $T_{1\mathrm{GM}}$ = 1711ms and $T_{1\mathrm{blood}}$ = 1711ms.

The transit delay was assumed to be 379ms, with an inversion efficiency of 95%, λ for GM of 0.98 and λ for WM of 0.82. These values were based on previous studies using this sequence on a 3T field [4].

For the 9.4T measurements, further testing using the FAIRPRESS sequence would have to be done to determine the equivalent parameters applicable at this field strength. Therefore, only the relative ΔM was calculated for the results' analysis (below, on section 6.4.1 of this thesis), avoiding the calculation of absolute quantified perfusion values. This also applies to the T_2* quantification and analysis.

4.7.1 Sequence Optimization

The analysis of the results was performed using Microsoft Excel 2007 (Microsoft, Redmond, Washington). In order to compare multiple results from the reconstructions, a one-way analysis of variance (ANOVA) was performed on MATLAB, with the Statistical Toolbox, with the help of in-house functions.

4.7.1.1 Reconstruction optimization

Different reconstruction methods for calculating ΔM were tested with respect to their influence on the signal stability and SNR. The results attained for each method were termed absFID, complFID, absSpec and complSpec. The first two used the signal amplitude after exponential fitting of the FIDs to calculate the difference between tag and control and determine ΔM. The Spec methods applied a FT to the data, and then calculated the difference of the integral of the tag and control spectra, for the predetermined central water peak points. Their differences are as follows:

- **absFID**: the data was first magnitude-combined and then averaged;
- **complFID**: the data was first averaged, phase corrected and then complex combined;
- **absSpec**: the data was first exponentially filtered and an Fourier transformed. The resulting spectra were magnitude-combined and then averaged;
- **complSpec**: the data was first averaged, phase corrected and complex combined. It is then exponentially filtered and Fourier transformed, and then magnitude-combined.

Additional variations in which the averaging was performed before combining the coil signals yielded equal results, and were therefore discarded.

4.7.2 Functional Studies

All the analyses, both statistical and qualitative, were done using MATLAB, with home-made routines. In order to compare matched pairs of data, Student's paired sample t-tests were performed using MATLAB's Statistical Toolbox.

4.7.2.1 T_2* reconstruction optimization

The T_2* corresponds to the decay rate of the FID, as seen in Eq. 3 and Fig. 3. It is possible to obtain this value by fitting an exponential to the data and calculating this decay rate. This was done by using MATLAB's Curve Fitting Toolbox. In order to determine if there was an optimal reconstruction for the T_2* data, two different possibilities were tested:

- **absFIDT2s**: uses the absFID data (after being magnitude-combined and averaged) for the exponential fit;
- **complFIDT2s**: uses the complFID data (after being averaged, phase corrected and then complex combined) for the exponential fit.

Chapter 5
Sequence Optimization

This chapter includes the initial optimization of the FAIRPRESS sequence, as well as the testing and comparison of PCASLPRESS, FAIRPRESS and FAIRPRESS with BS perfusion measurements. The different reconstructions tested are also evaluated here. The analysis of the obtained results is also included.

5.1 FAIRPRESS optimization

Different parameters were tested, including pre-saturation, ISF, *TI* and a relaxation delay before each acquisition (waiting for a short time before running the sequence), while measuring perfusion in the CC during rest. The relative magnetization difference was assessed, as a relative perfusion measurement. Previous results for relative perfusion measurements in WM using this sequence found a ΔM value of around 0.1%. The stability of the results obtained with the different parameters was analyzed, and the ones that showed the most stable results were chosen.

No pre-saturation, an ISF of 3.0, a relaxation delay before each acquisition and a *TI* of 1500ms (Fig. 36) were the parameters that yielded the best results, and were thus chosen for the following experiments.

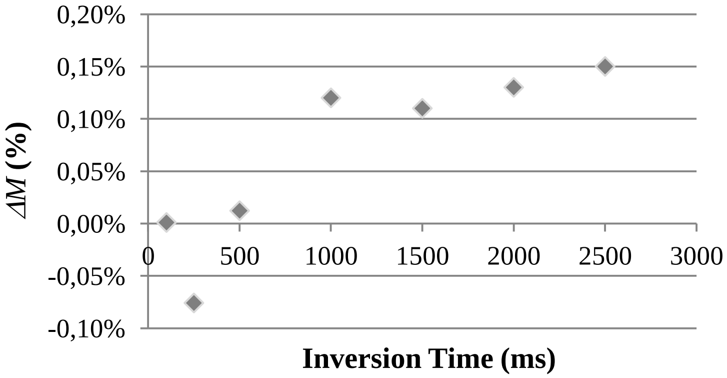

Figure 36 – Relative magnetization difference in function of *TI*, measured in the CC for a single subject.

5.1.1 Reconstruction optimization

In order to analyze the results, the mean of the resulting relative perfusion values without averaging was calculated, as well as the standard deviation, for every acquisition and reconstruction. The SNR was calculated as the mean of the relative perfusion measurements divided by the standard deviation. The different results were then compared within each subject, for the different acquisitions (WM, GM, ventricle and no perfusion). Finally, the results were grouped for each sequence and for each acquisition (example depicted in Table 6), and an intersubject analysis was done, calculating the mean value of ΔM, standard deviation and SNR. The different reconstructions were then evaluated based on this information.

Table 6 – Mean intersubject SNR analysis for FAIRPRESS with background suppression, for the different reconstructions, in white matter.

Subject	AbsSpec	ComplSpec	AbsFID	ComplFID
1	0.801	0.794	0.352	0.735
2	0.476	0.471	0.344	0.373
3	2.084	2.065	2.891	1.864
4	0.192	0.196	0.304	0.202
5	0.361	0.340	0.509	0.345
6	0.747	0.697	0.856	0.673
7	1.099	1.094	1.371	1.028

A One-Way ANOVA was applied to the different reconstructions' SNR values, in all subjects for each sequence (as presented in Table 6), and separately for WM and GM. The results showed that there was not a significant difference between the different reconstructions (Table 7), all of them being equivalent. Therefore, it was decided to use the value that was the computationally easiest to calculate, the absSpec, for the reconstruction and subsequent CBF calculations.

Table 7 – One-Way ANOVA test results, for WM and GM and the different sequences.

	WHITE MATTER		GREY MATTER	
Sequence	**p-value**	**Significantly ≠?**	**p-value**	**Significantly ≠?**
FAIRPRESS	0.87	No	1.00	No
FAIRPRESS BS	0.96	No	0.69	No
PCASLPRESS	1.00	No	1.00	No

5.1.2 Sequences

The comparison among the three sequences, FAIRPRESS without BS, FAIRPRESS with BS and PCASLPRESS, was done after obtaining the absSpec mean values, standard deviation and SNR for each sequence and for each acquisition, for the 7 subjects tested. Each sequence's SNR error was calculated as the standard deviation of the SNR for each subject.

Table 8 – Relative magnetization difference and SNR from the intersubject analysis, for the three sequences in GM.

	FAIRPRESS no BS	FAIRPRESS BS	PCASLPRESS
ΔM (%)	0.493 ± 0.268	0.375 ± 0.262	0.049 ± 0.353
SNR	1.729 ± 0.652	2.188 ± 0.959	0.959 ± 0.663

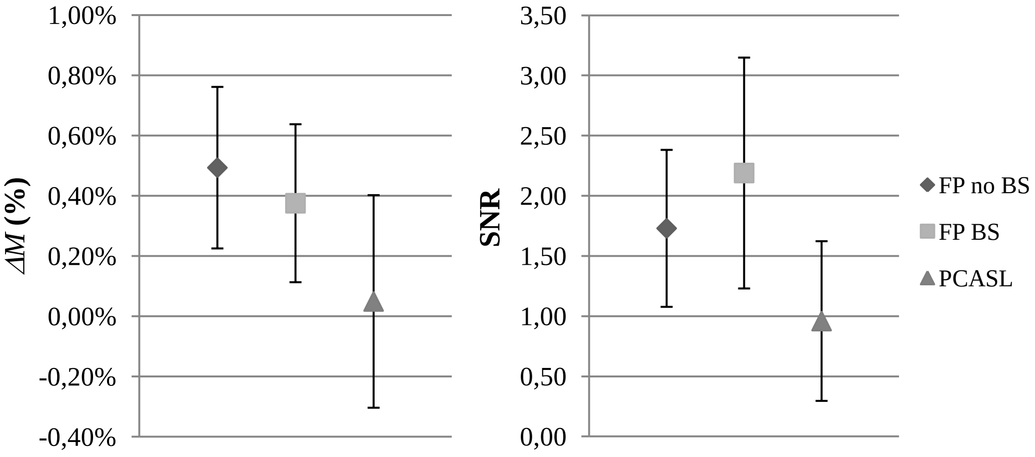

Figure 37 – Comparison between the three sequences for measurements in GM, regarding relative perfusion (**left**) and SNR (**right**).

For measurements in GM (Table 8 and Fig. 37), there were no significant differences between sequences. Although the mean relative perfusion value for FAIRPRESS without BS was slightly larger than with BS, the mean SNR for FAIRPRESS with BS was higher. PCASLPRESS yielded the worst results.

Table 9 – Relative magnetization difference and SNR from the intersubject analysis, for the three sequences in WM.

	FAIRPRESS no BS	FAIRPRESS BS	PCASLPRESS
ΔM (%)	0.187 ± 0.091	0.147 ± 0.068	0.058 ± 0.116
SNR	0.569 ± 0.281	0.823 ± 0.633	0.257 ± 0.298

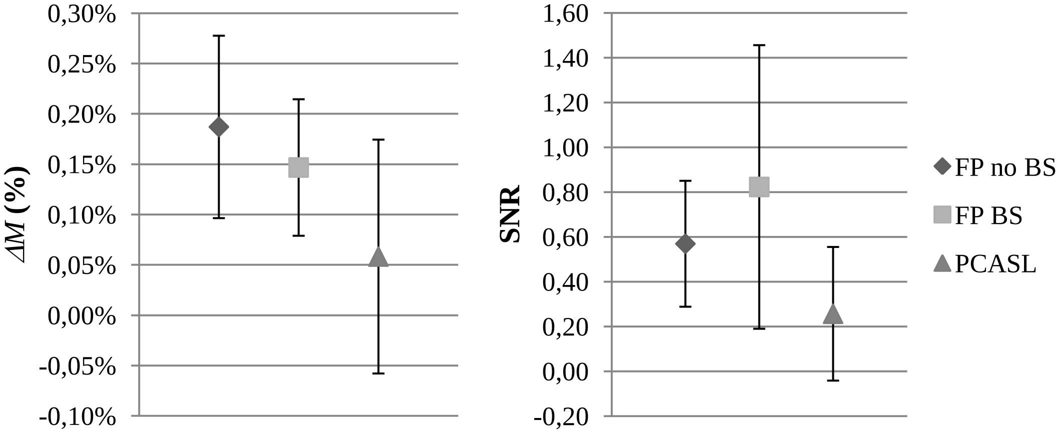

Figure 38 – Comparison between the three sequences for measurements in white matter, regarding relative perfusion (**left**) and SNR (**right**).

For measurements in WM (Table 9 and Fig. 38) – the tissue that is the main object of our study – there were again no significant differences between sequences. The mean relative perfusion value for FAIRPRESS without BS was slightly higher than with BS and the mean SNR for FAIRPRESS with BS was the highest. PCASLPRESS showed the worst results again.

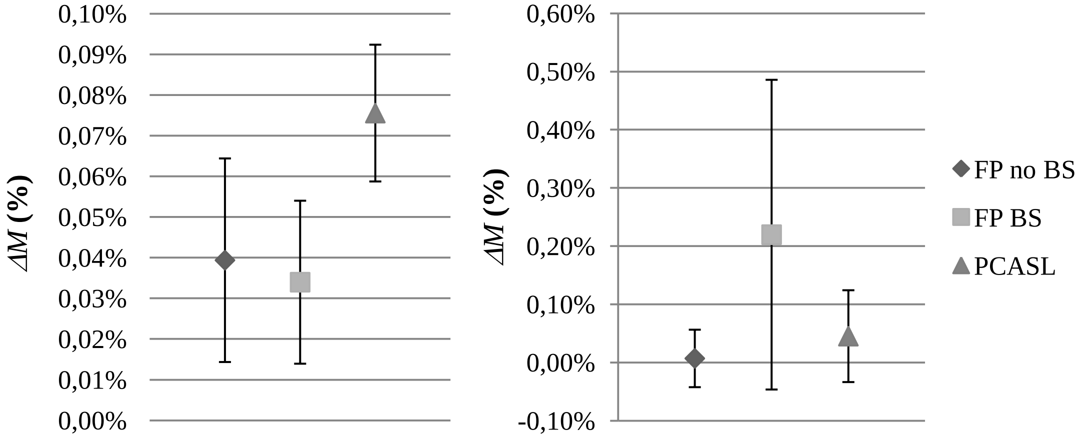

Figure 39 – Relative perfusion comparison between the three sequences for measurements in the ventricle (**left**) and without perfusion labeling (**right**).

The control experiments (Fig. 39), in situations where there was supposed to be no perfusion signal, showed similar results for all the sequences, being that their values' interval include zero or are very close to it. PCASLPRESS in the ventricle showed slightly higher results than expected, which in conjunction with the results presented above in GM and WM, might indicate a problem in the sequence implementation.

FAIRPRESS with BS, supposedly without perfusion labeling when using an ISF of 99.9, displayed a high mean value of perfusion with a large standard deviation. The causes for this are not clear, however, considering the overall good results of the sequence, even when measuring in the ventricle, this factor did not have a big impact in this sequence's evaluation.

Chapter 6
Functional Studies

In this chapter, the results of the functional studies performed are presented and analyzed, for both the visual stimulus and the adapted Poffenberger task, at a magnetic field of 3T and 9.4T. The results of the T_2* reconstruction optimization are also presented.

6.1 General considerations

For the stimulus experiments, extreme perfusion outliers, probably associated with subject motion during the scan, were removed by using a threshold of three times the interquartile range above the third quartile or below the first quartile, for all perfusion measurements. These values were replaced by the mean of the immediately prior and following values, or if the outlier was in the boundary between two states, the mean of the two previous values (example depicted on Fig. 40).

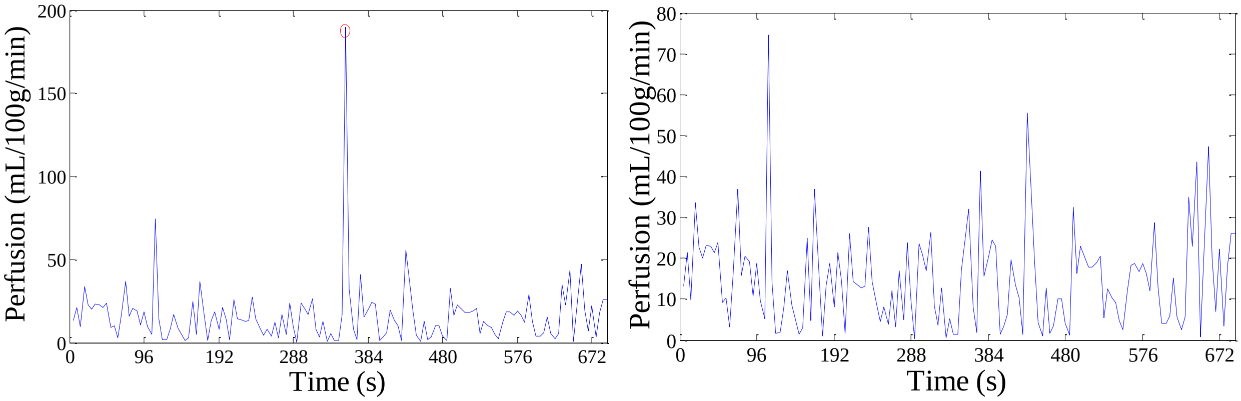

Figure 40 – Left: Data acquired during a measurement in the *corpus callosum*, with an outlier probably due to motion circled in red (Subject 5 in the Poffenberger Task experiments). **Right**: Same dataset, after outlier removal.

For the Student's paired sample t-test analysis, as well as for the graphical representation of the averaged data, the response delay to stimulation, which can reach 8s in CC activation [58] but lies between 1 and 2s in the GM (Fig. 13), was taken into account. Therefore, the points used for further analysis were the ones acquired after approximately 10s for WM and 4s for GM after the beginning of each state.

The significance level considered for these studies' statistical analysis was 0.05, meaning that statistical significance is only achieved when the p-value is under 0.05.

Given the exploratory nature of the analysis and the multiple comparisons performed, usage of the Bonferroni correction was considered. This would imply lowering the significance level by dividing it by the number of comparisons performed. This correction is applied to take into account the increased possibility of type-I error when there are multiple comparisons being performed simultaneously, controlling for false positives. However, this correction also increases the risk of generating false negatives (type-II errors) and its use was therefore discarded [59].

For the percentage change analysis of the differences between the activation and rest states, the average of the considered data points for both the T_2* and perfusion measurements was calculated. Then, the subtraction of these averaged values was done (activation minus rest), and the result was turned into a percentage of the average of the activated state – the percentage change. Therefore, a positive change means that the activated state has a larger value than the rest state, and a negative change the opposite. In order to normalize the percentage change, all dataset values were increased by the absolute of the minimum value, so that all values were positive while the changes between them remained the same.

6.2 Visual stimulus

6.2.1 T_2* reconstruction optimization

In order to analyze the results, the mean of the resulting relative perfusion values during rest, without averaging was calculated, as well as the standard deviation, for every acquisition and reconstruction. The SNR was calculated as the mean divided by the standard deviation. The two different reconstructions were then evaluated.

Table 10 – Mean intersubject SNR analysis for FAIRPRESS without BS, for the two reconstructions, in the CC and only for the rest state.

Subject	absFIDT2s	complFIDT2s
1	194.51	192.91
2	100.29	102.44
3	139.26	138.84
4	102.60	101.21
5	111.99	112.66
6	155.89	144.97
7	144.44	120.99
8	174.18	153.30
9	96.04	95.42

A Student’s paired sample t-test was applied to the different reconstructions’ SNR results, in all subjects for the CC (Table 10). The results showed that there was no significant difference between the reconstructions (p-value = 0.08). However, this result was close to significance and showed that absFIDT2s had a generally higher SNR. Considering that this value was also computationally easier to calculate, the absFIDT2s was chosen for determining the T_2* for the visual stimulus experiments.

6.2.2 Results

In GM measurements in the VC, the difference between the rest and activation states was predominantly very significant, for both the perfusion and T_2* values. This is clear even without averaging the data, as depicted in Fig. 41. It is also interesting to note the clear presence of the previously mentioned T_2* drift, that commonly affects BOLD acquisitions, which does not affect the simultaneous perfusion measurements (Fig. 41).

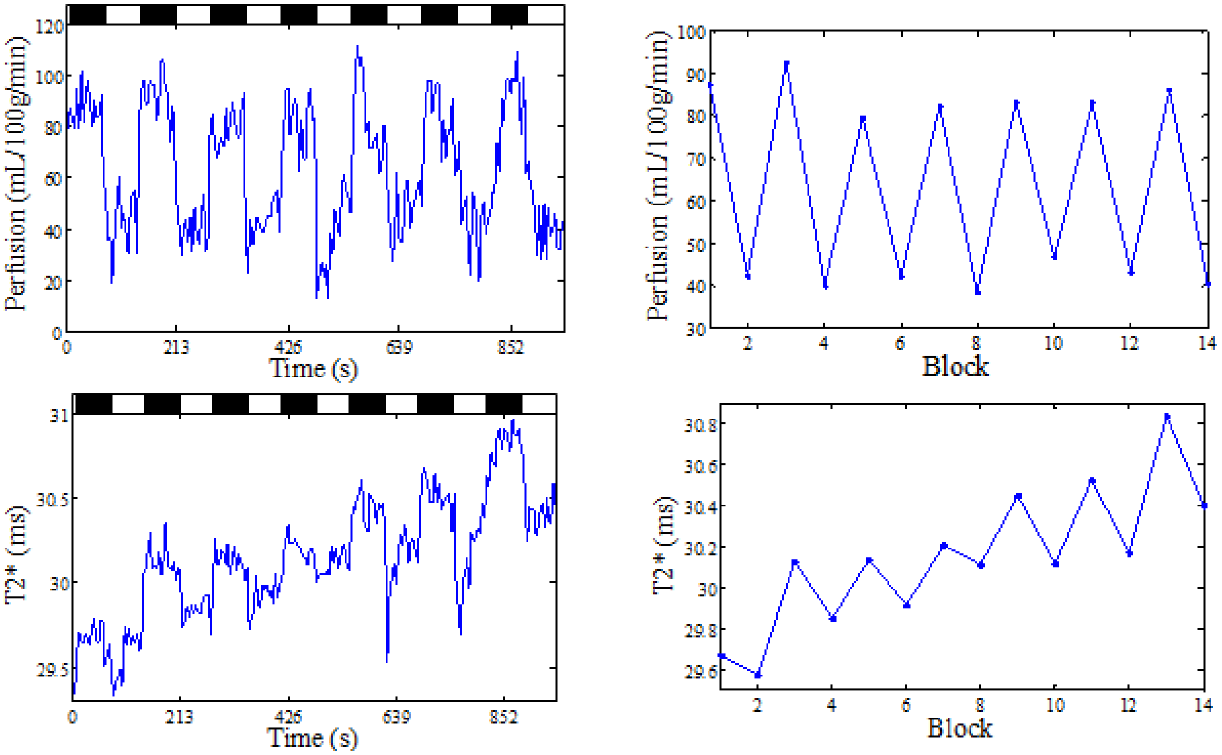

Figure 41 – **Left**: Perfusion and T_2* signals, acquired simultaneously for subject 1, in the GM. Above the graphics, the stimuli periods are represented in black and the rest periods in white. **Right**: Corresponding averaged data, where one point translates one state and also disregarding the points acquired during the activation delay considered for GM.

In the WM, the difference between rest and activation is not as clear as without averaging. Even after averaging, not all points seem to have a dependency on the state (rest or activation). This can be seen for both the CC and the VC, in Figs. 42 and 43, respectively.

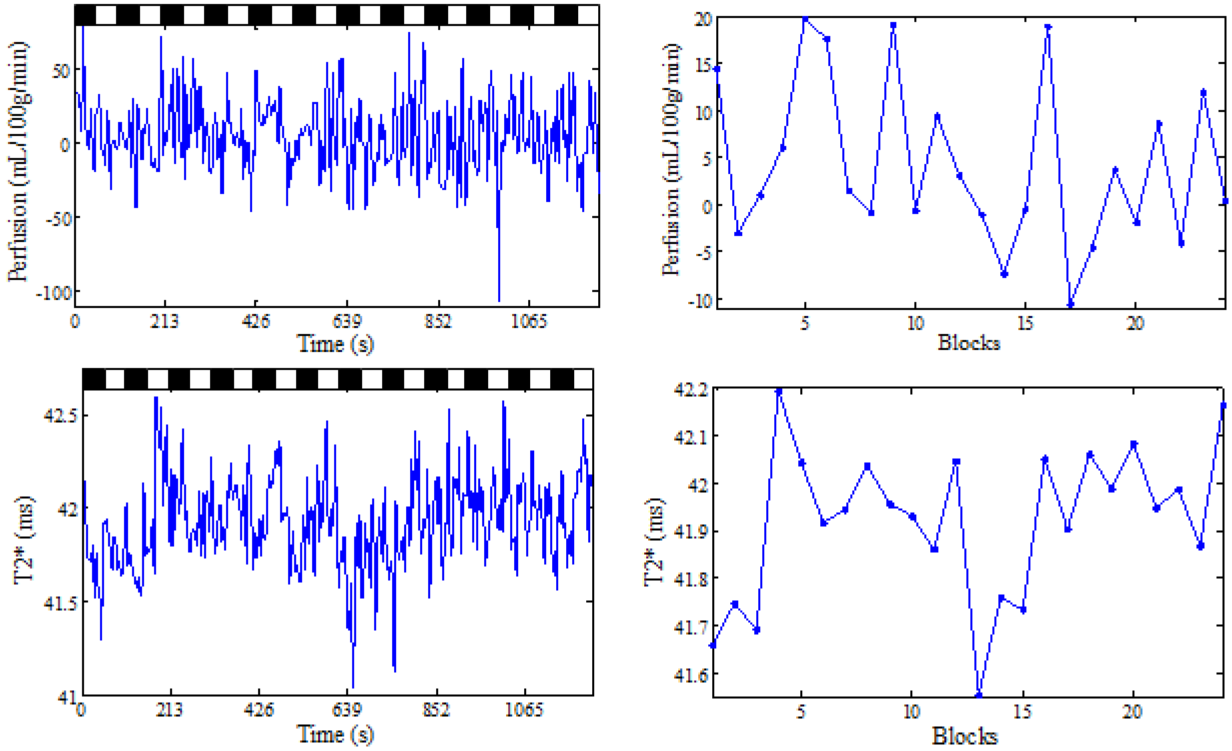

Figure 42 – **Left**: Perfusion and T_2* signals, acquired simultaneously for subject 8, in the CC. Above the graphics, the stimuli periods are represented in black and the rest periods in white. **Right**: Corresponding averaged data, where one point translates one state and also disregarding the points acquired during the activation delay considered for WM.

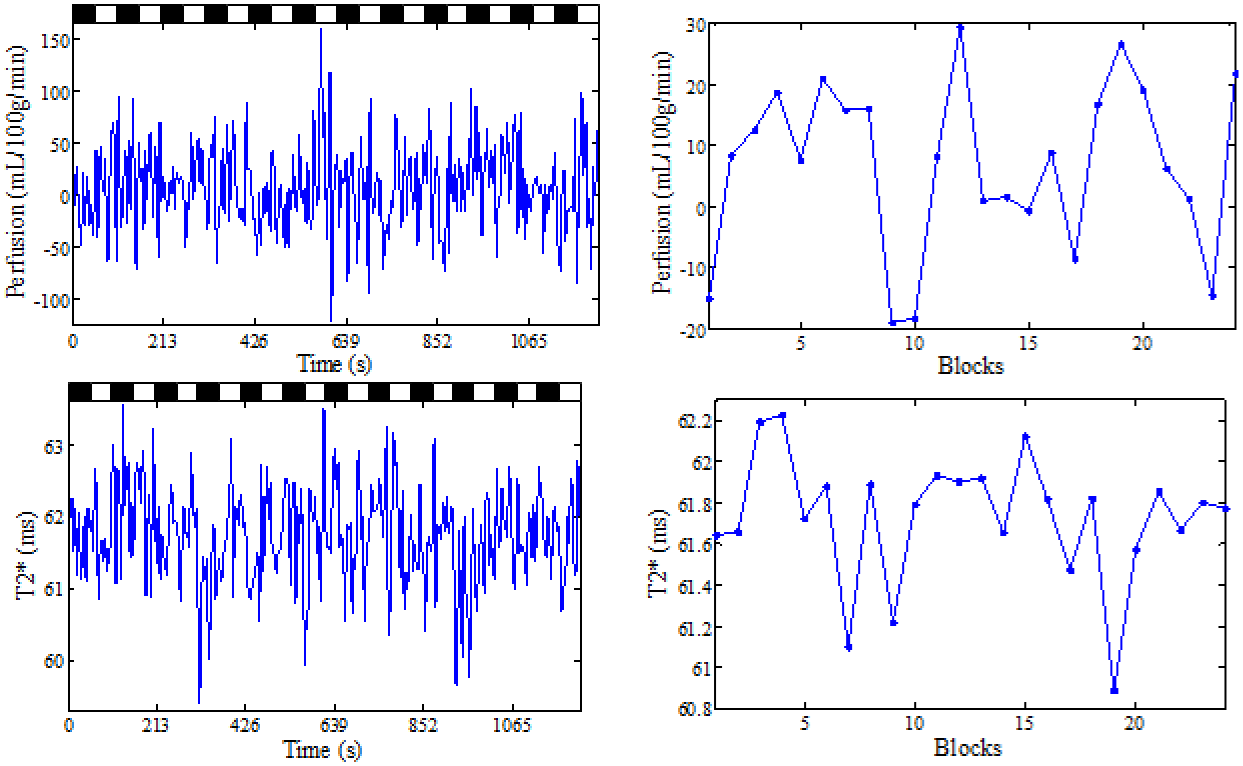

Figure 43 – Left: Perfusion and T_2* signals, acquired simultaneously for subject 6, in the VC. Above the graphics, the stimuli periods are represented in black and the rest periods in white. **Right**: Corresponding averaged data, where one point translates one state and also disregarding the points acquired during the activation delay considered for WM.

After this qualitative analysis, Student's t-tests were performed for each data set, to test if the perfusion and T_2* measurements acquired during stimulation were significantly different from the ones acquired during rest. The percentage change from the average of all the stimulus states to the average of all the rest states, per subject and per tissue, was also calculated and used in the comparison (Table 11).

Table 11 – Student's t-test and percentage change results for the different subjects in grey matter.

		PERFUSION				T_2*			
Acquisition	**Subject**	**p**	**Activation ≠ Rest (95% conf.)**	**Close to being ≠ (70% conf.)**	**Change (%)**	**p**	**Activation ≠ Rest (95% conf.)**	**Close to being ≠ (70% conf.)**	**Change (%)**
Single	**1**	<0.01	Different	Close	44.11	<0.01	Different	Close	0.86
	2	0.30	Not Different	Close	3.69	0.51	Not Different	Not Close	-0.11
	3	<0.01	Different	Close	28.93	<0.01	Different	Close	2.58
	4	0.02	Different	Close	15.85	<0.01	Different	Close	0.92
	5	<0.01	Different	Close	16.10	<0.01	Different	Close	1.32
	6	<0.01	Different	Close	46.34	<0.01	Different	Close	4.16
	7	<0.01	Different	Close	28.45	<0.01	Different	Close	1.03
	8	0.22	Not Different	Close	9.07	<0.01	Different	Close	0.25
	9	0.08	Not Different	Close	11.90	0.16	Not Different	Close	0.26

In GM, 6 out of 9 subjects showed a significant difference between the activation and rest states, and one other had a result close to significance (considered at a 90% confidence level), regarding perfusion. For T_2*, in 7 out of 9 subjects the differences between states were significant, and for one other subject the result was also close to significance. A probable explanation for the subjects where this difference was far from significance is that the voxel positioning was not accurately placed in an activated area of GM. Therefore, these subjects were not included in further analysis.

The percentage change between activation and rest was much larger for the CBF values than T_2*. The values obtained for both are in accordance with previous findings in GM [60].

When the difference was significant, the change value was generally also larger, which was to be expected. It is also interesting to note that in 8 out of the 9 of subjects, both T_2* and perfusion behaved similarly, considering a "tendency" threshold with 70% confidence. For the only subject where this did not happen, the percentage change was also the lowest achieved. These results might indicate a generally good placement of the voxel and overall measure of neural activation, using this technique in GM.

Table 12 – Student's t-test and percentage change results for the different subjects in the CC.

		PERFUSION				T_2*			
Acquisition	**Subject**	**p**	**Activation ≠ Rest (95% conf.)**	**Close to being ≠ (70% conf.)**	**Change (%)**	**p**	**Activation ≠ Rest (95% conf.)**	**Close to being ≠ (70% conf.)**	**Change (%)**
Single	**1**	0.75	Not Different	Not Close	1.69	<0.01	Different	Close	0.19
	2	1.00	Not Different	Not Close	0.01	0.89	Not Different	Not Close	0.02
	3	0.52	Not Different	Not Close	-1.35	0.63	Not Different	Not Close	0.05
	4	0.44	Not Different	Not Close	3.43	<0.01	Different	Close	-0.40
	5	0.62	Not Different	Not Close	-0.26	0.50	Not Different	Not Close	0.09
Double	**6**	0.86	Not Different	Not Close	-0.66	1.00	Not Different	Not Close	<0.01
	7	0.35	Not Different	Not Close	-0.80	0.63	Not Different	Not Close	-0.04
	8	0.16	Not Different	Close	0.76	<0.01	Different	Close	-0.36
	9	0.18	Not Different	Close	-0.48	0.86	Not Different	Not Close	-0.02

On the contrary, in the CC (Table 12), there were no significant differences between rest and stimulation regarding the perfusion measurements. Even so, it was possible to see a tendency towards difference in 2 out of the 9 subjects analyzed (with a confidence level of over 70%).

The T_2* results were very significant for 1/3 of the subjects. In this case, only subject 8 showed similar results between perfusion and T_2*, regarding the t-test, which might indicate good voxel positioning in this case. The generally poor results obtained might be explained by overall poor voxel positioning in the specifically activated area of the CC. The number of acquisitions also had an impact in the results, since both the results closer to significance in the perfusion measurements were achieved for the double acquisition experiments.

For two of the three significant results with T_2*, the change was negative, meaning that the activated state had lower T_2* than the rest state. This effect has been previously reported in the literature [61, 62]. Three possible explanations for this phenomenon have been theorized:

1. "Vascular steal", which is based on the concept that there is a fixed amount of oxygenated blood at a time, and as some of it is diverted to active areas, the neighboring areas would then show a negative BOLD signal [61];
2. Active neural suppression, which says that certain areas can have reduced functional activity below the baseline during a particular stimulus [61];
3. Extension of the "initial dip", which states that there is actually an increase in neural activity during the stimulus, but there is not the corresponding expected CBF increase. The activation would then exhaust the local oxygen levels, resulting in an extension of the "initial dip" (Chapter 1, Functional MRI, Fig. 12) [61]. Another

> study's results suggest that the initial dip and the prolonged negative BOLD response have different origins and characteristics. The same study indicates that a decrease in CBF can be explained by the reduction or suppression of neural activity, or the previously explained "vascular steal" effect, as seen in previous studies [62].

Considering the case where there was a significant T_2* difference between states and close to significance for the perfusion values (Subj. 8), the observed change values were positive for perfusion and yet, negative for T_2*. In this case, the initial dip explanation would not fit, corroborating the results seen in [62].

Considering that the voxel was placed in the same structure and in the same region in all subjects, the active neural suppression theory seems unlikely, but since voxel positioning was not exactly the same for all subjects, it also cannot be ruled out. The "vascular steal" theory also seems unlikely based on these results, since the simultaneous CBF change was positive.

The previously mentioned better spatial localization of ASL when compared with BOLD for fMRI studies may also account for this phenomenon, since ASL measurements are more weighted toward arteries and BOLD toward veins. For this reason, it is possible that the voxel is actually placed in an active area, showing a positive perfusion change, but since the BOLD signal localization is slightly deviated, it shows a negative value, possibly indicating an adjacent active area.

Regarding subject 4, who shows a very significant T_2* difference between states, but not for the perfusion measurements, the percentage changes showed the same tendency as for subject 8 (being also the highest observed), so the same conclusions might be extrapolated for this case.

The reason why some results do not show a similar behavior between both perfusion and T_2*, being significant for one but not the other, is also not clear. For those particular acquisitions, it is possible that either measurement became more unstable than the other. For example, BOLD is more affected by bad shimming than ASL, and ASL is more affected by subject motion (for example, due to breathing) since the subtraction for perfusion calculation would then be unstable. The previously explained slight deviation between ASL and BOLD measurements might also account for this phenomenon, if that deviation is large enough to not even be adjacent to the activated region.

Table 13 – Student's t-test and percentage change results for the different subjects in the WM of the VC.

		PERFUSION				T_2*			
Acquisition	**Subject**	**p**	**Activation ≠ Rest (95% conf.)**	**Close to being ≠ (70% conf.)**	**Change (%)**	**p**	**Activation ≠ Rest (95% conf.)**	**Close to being ≠ (70% conf.)**	**Change (%)**
Single	**5**	0,79	Not Different	Not Close	-1.33	0.18	Not Different	Close	0.14
Double	**6**	0,07	Not Different	Close	8.91	<0.01	Different	Close	0.39
	7	0,08	Not Different	Close	7.30	0.46	Not Different	Not Close	0.08
	8	0,38	Not Different	Not Close	3.84	0.10	Not Different	Close	0.30
	9	0,04	Different	Close	-8.50	0.07	Not Different	Close	-0.24

In the WM of the VC (Table 13), the perfusion measurements showed significant differences between the rest and activation states for one subject (9), and very close to significance in two others (6 and 7).

The T_2* showed a significant difference for one subject and close to significance differences for three others. It behaved similarly to perfusion in 2/5 of the cases.

It is important to note that these measurements are much more prone to partial volume effects than the measurements in deep WM, like in the CC, due to WM's proximity to GM in the VC and the voxel's size and positioning (even with the extra care taken, described in Chapter 4).

For subjects 6 and 9, who had similar results for T_2* and perfusion and also significant or very close to significance differences in both cases, there was a correlation between positive change (6) and negative change (9) for T_2* and perfusion. The percentage change observed was also the highest for both these subjects, which might also be indicative of good voxel positioning.

The negative results might be explained by both the vascular steal and neural activation suppression theories, previously explained regarding the CC observations. The results that do not show similar behavior between T_2* and perfusion might also have the same explanation as previously presented for the measurements in the CC.

Again, the results seem to have been improved by acquiring twice for the same voxel position, as intended.

6.3 Adapted Poffenberger task (3T)

6.3.1 T_2* reconstruction optimization

After analyzing the exponential fitting based on absFID and complFID, as previously done on section 6.1.1 of this thesis, the results observed for absFIDT2s on the background suppressed data were not viable.

When there is no signal, there is still noise oscillating around zero. Since with absFID the magnitude of the data is taken, this noise is all made positive, and averaging after this generates a relatively strong offset (Fig. 44, left). Considering that the background suppressed data has a naturally lower maximum signal, the fit tries to keep up with the offset for a longer time, making the fit result unusable for calculating T_2* .

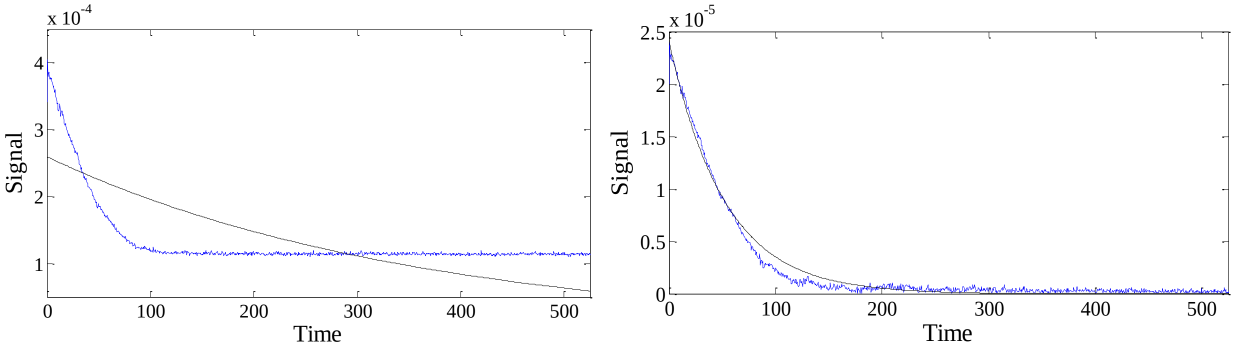

Figure 44 – Left: absFID reconstructed signal (blue) and the corresponding fit result (black). **Right**: complFID reconstructed signal (blue) and the corresponding fit result (black). Both graphs show background suppressed data from the same measurement in the CC.

Therefore, for the data acquired using FAIRPRESS with BS, the T_2* reconstruction used was complFIDT2s, which is not affected by this offset, for calculating the T_2* results (Fig. 44, right). As is particularly visible in the graph on the right of Fig. 44, a single exponential fit does not yet seem to be optimal for the signals acquired in the WM. However, by using MATLAB's Curve Fitting Toolbox to test other fit functions (single and double exponentials, as well as Gaussian functions), none proved to be better than the single exponential fit used in this thesis.

6.3.2 Results

In order to confirm if by using the adapted Poffenberger task and FAIRPRESS with BS the results in GM remained acceptable, one experiment in one subject was performed by placing the voxel in GM of the VC.

Table 14 – Student's t-test and percentage change results for subject 1, in grey matter.

		PERFUSION				T_2*			
Acquisition	**Subject**	**p**	**Activation ≠ Rest (95% conf.)**	**Close to being ≠ (70% conf.)**	**Change (%)**	**p**	**Activation ≠ Rest (95% conf.)**	**Close to being ≠ (70% conf.)**	**Change (%)**
Single	**1**	<0.01	Different	Close	39.75	<0.01	Different	Close	3.96

Regarding the qualitative analysis, the difference between states seems clear, for both T_2* and perfusion, again, even without averaging (results not shown). By doing the statistical analysis, for both T_2* and perfusion, the difference between rest and activation was very significant, and the percentage change for both was quite high, as expected for GM (Table 14).

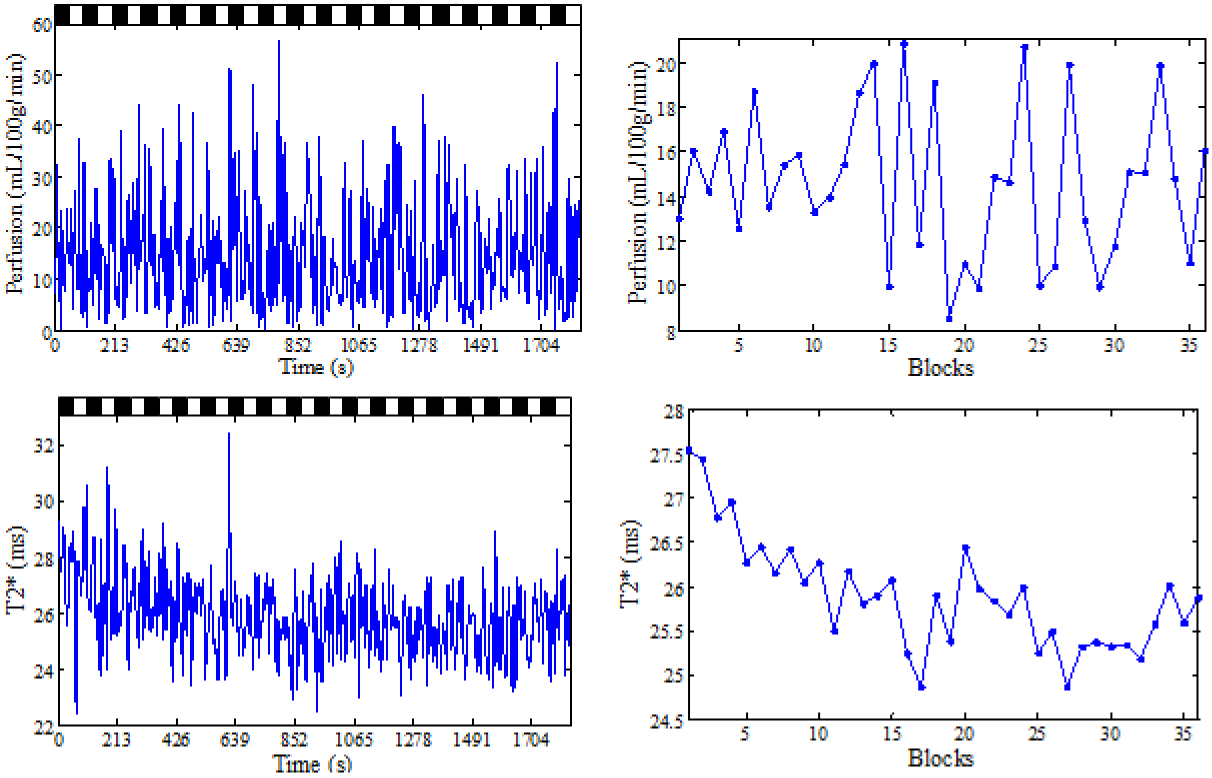

Figure 45 – Left: Perfusion and T_2* signals, acquired simultaneously for subject 8, in the CC. Above the graphics, the stimuli periods are represented in black and the rest periods in white. **Right**: Corresponding averaged data, where one point translates one state and also disregarding the points acquired during the activation delay considered for WM.

Table 15 – Student's t-test and percentage change results for the different subjects in the CC.

		PERFUSION				T_2*			
Acquisition	**Subject**	**p**	**Activation ≠ Rest (95% conf.)**	**Close to being ≠ (70% conf.)**	**Change (%)**	**p**	**Activation ≠ Rest (95% conf.)**	**Close to being ≠ (70% conf.)**	**Change (%)**
Double	**1**	0.82	Not Different	Not Close	-1.96	<0.01	Different	Close	-2.39
Triple	**2**	0.86	Not Different	Not Close	1.33	0.67	Not Different	Not Close	-0.21
	3	0.95	Not Different	Not Close	-0.47	0.52	Not Different	Not Close	0.21
	4	0.97	Not Different	Not Close	-0.34	0.90	Not Different	Not Close	0.07
	5	0.20	Not Different	Close	-10.16	0.21	Not Different	Close	-0.60
	6	0.94	Not Different	Not Close	0.54	0.02	Different	Close	-0.86
	7	0.15	Not Different	Close	10.11	0.64	Not Different	Not Close	0.22
	8	0.06	Not Different	Close	-17.03	0.09	Not Different	Close	-0.89

Again, for the perfusion measurements in the CC, there were no significant changes between activation and rest for any of the subjects (Fig. 45 and Table 15). Even so, 3 out of the 8 subjects showed results close to significance (with a confidence level of 80% or more).

For T_2*, 2 out of 8 subjects showed a significant difference between rest and activation, and 2 others showed results close to significance.

Comparing these results to the ones acquired with the FAIRPRESS without BS and with the visual stimulus in the CC, there was an overall improvement of the number of close to significance cases (from 22% to 37.5% with perfusion and from 33% to 50% with T_2*).

Only subjects 8 and 5 showed similar t-test results between perfusion and the T_2*, which might indicate better voxel placement in these cases. For these subjects it is also possible to see some of the highest percentage change between rest and activation, for both T_2* and perfusion. There also exists a correlation between the sign of these changes, both being negative for both subjects as well. These negative changes may again be explained by the vascular steal and neural activation suppression theories, previously presented in section 5.2.1.

6.4 Adapted Poffenberger task (9.4T)

6.4.1 Results

A measurement was performed in a voxel in the GM of the VC, in order to test it at higher field strength. The statistical analysis results are presented on Table 16.

Table 16 – Student's t-test and percentage change results for subject 1, in grey matter.

		PERFUSION				T_2*			
Acquisition	**Subject**	**p**	**Activation ≠ Rest (95% conf.)**	**Close to being ≠ (70% conf.)**	**Change (%)**	**p**	**Activation ≠ Rest (95% conf.)**	**Close to being ≠ (70% conf.)**	**Change (%)**
Single	**1**	0.24	Not Different	Close	8.28	<0.01	Different	Close	-14.92

The results regarding perfusion were not as expected for a GM voxel, since they were not significant, although close, considering the 70% confidence level. However, for T_2* there was a very significant difference between rest and activation ($p<0.01$).

It is thus possible that the voxel was placed close to an activated region. This is also corroborated by the percentage changes having different signals, associated with the vascular steal theory, presented above.

At higher field strengths, it is also possible that the previously mentioned instabilities, that might affect BOLD and ASL differently during the same acquisition might also be exacerbated, originating differences as the ones observed.

A dual acquisition experiment was then performed on the CC, for two subjects. The graphical result for one of the subjects is presented in Fig. 46, while the statistical analysis results for both subjects are presented in Table 17.

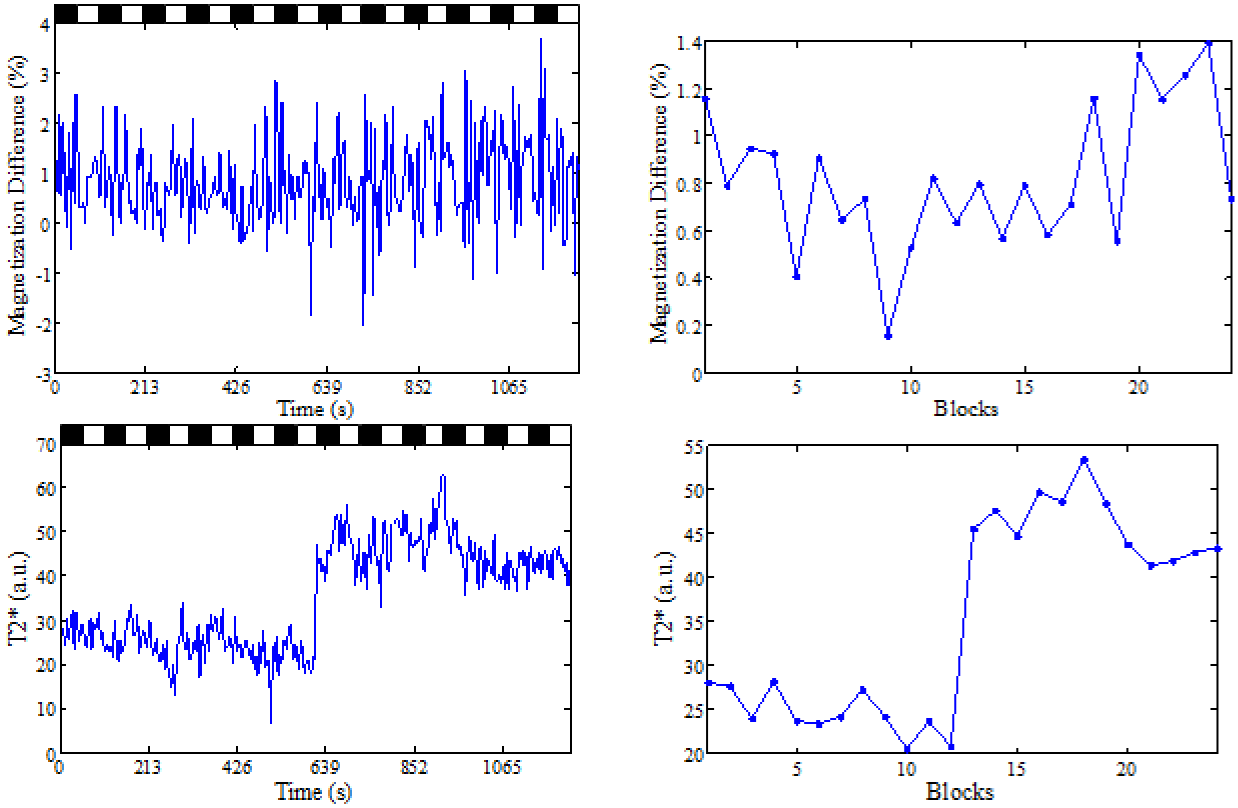

Figure 46 – Left: Perfusion and T_2* signals, acquired simultaneously for subject 1, in the CC. Above the graphics, the stimuli periods are represented in black and the rest periods in white. **Right**: Corresponding averaged data, where one point translates one state and also disregarding the points acquired during the activation delay considered for WM.

Table 17 – Student's t-test and percentage change results for the different subjects in the CC.

		PERFUSION				T_2*			
Acquisition	**Subject**	**p**	**Activation ≠ Rest (95% conf.)**	**Close to being ≠ (70% conf.)**	**Change (%)**	**p**	**Activation ≠ Rest (95% conf.)**	**Close to being ≠ (70% conf.)**	**Change (%)**
Double	**1**	0.64	Not Different	Not Close	-1.74	0.26	Not Different	Close	-1.26
	2	0.88	Not Different	Not Close	0.72	<0.01	Different	Close	6.69

Regarding the qualitative analysis, the difference between activation and rest states is not clear for all data points, even after averaging, for neither perfusion or T_2*.

There were no significant differences regarding the perfusion measurements, however T_2* showed one significant result and one close to significance. Again, this may mean that the change in perfusion is much weaker than the T_2*'s, or even nonexistent. Other possible explanations are some instability, related to the ASL acquisition, or maybe a slight deviation from the activated region of the CC.

Something that is quite clear in these results is one of the advantages of ASL fMRI when compared to BOLD fMRI – the baseline variation that affects the T_2* does not affect the perfusion measurements. It is possible to see that from block 12 to 13 for the averaged T_2* results in Fig. 46, where the transition between acquisitions happens, there is a signal baseline “jump”. It is also important to note that between these acquisitions only a quick FLASH 2D was performed, to assess subject movement. At the 9.4T field there is a high sensitivity for T_2*, therefore even slight subject motion, resulting in a slightly different voxel position for the second scan, could cause a large effect as the one seen in Fig. 46, while at the 3T field it would not be visible.

The percentage change between states was also quite large, when compared to the previous results. This might be explained by the higher sensitivity derived from the higher magnetic field strength used in this experiment. However, the possibility of a higher signal due to external contributions (since the saturation around the voxel was not as good as the previous experiments in the 3T field) cannot be disregarded.

Chapter 7

Conclusions and Future Work

Regarding sequence optimization, FAIRPRESS with BS yielded the best results. However, since the disappointing results obtained with the PCASLPRESS sequence are expected to be due to a still unidentified implementation issue, further studies should be done in order to test the efficiency of this sequence for measuring perfusion in WM. It is also important to note that both BS and PCASL are currently not applicable at higher magnetic field strengths like 9.4T, due to SAR limitations.

In addition, both the sequences and the data reconstruction and analysis can still be improved to obtain more significant results.

The technique used in this dissertation for perfusion measurements shows that by sacrificing spatial resolution in favor of sensitivity, it is possible to get quantified perfusion values with high accuracy, even in WM. The optimized sequences presented in this project could be used to characterize and investigate localized WM pathologies.

The functional experiments performed in this project showed great potential when measuring activation in GM. One possible future application would be to use this technique for real-time neurofeedback acquisition, of both T_2* and perfusion in the brain during stimulation. Functional single-voxel spectroscopy for real time studies has already been tested at 7T, showing promising results [63].

However, the results obtained for functional measurements in WM are not clear. The majority of the results do not show a significant difference between rest and activation in this tissue. Based solely on these results, it could be stated that the changes associated with activation in the brain, measured using the techniques described in this dissertation, are purely restricted to GM, as previous studies have suggested [7]. It might also mean that the perfusion changes in the CC due to activation are very low or simply non-existing, or might occur at a very different timing than the one speculated in these experiments.

However, for some subjects, a tendency for different perfusion and T_2* values between activation and rest was observed. This might imply that there may be other reasons why the observed change between states was not significant; one possible reason would be that the voxel was not correctly positioned in the specifically activated region of the CC. Even though previous studies demonstrate that this region is quite limited, they also show some inter-subject variation for activation inside that specific region. Therefore, future work could combine this technique with DTI tractography, in order to help in finding the best possible voxel position in the activated area of the CC.

Another possible reason for these results could be that the changes related to activation in the CC occur in a much smaller volume than the voxel used in this study. By using DTI, this issue could also be addressed, by identifying the appropriate voxel dimension in order to lessen the contribution from non-activated tissue inside the selected voxel.

Despite the different stimuli used throughout the project, it is possible that they were still not the best suited for the desired activation effect in the CC; this can also still be improved. Also, a larger sample size might have helped to observe the desired difference between rest and activation in WM. In the future the number of measurements can still be increased, but the acquisition time of the experiment must be taken into account.

The negative changes observed for both T_2* and perfusion during activation can be explained by the vascular steal and active neural suppression theories, presented above in Chapter 6. It is interesting to note that the majority of the results close to significance in the CC displayed these negative changes. A 2011 study on functional connectivity suggests a negative correlation between WM perfusion and GM activity [64], which could also be an explanation for these observations.

Ways to improve the stability of both T_2* and ASL signals would also be beneficial for future applications of the techniques described in this dissertation. An optimized implementation of this technique for ultra-high field could also help in attaining better results.

In spite of the unclear results for the activation experiments, the examined technique shows great potential for measuring perfusion in WM. Further investigations, also using this sequence, will be necessary for determining the behavior of white matter under activation.

References

[1] P. van Gelderen, J. d. Zwart and J. H. Duyn, "Pittfalls of MRI Measurement of White Matter Perfusion Based on Arterial Spin Labeling," *Magnetic Resonance in Medicine,* vol. 59, no. 4, pp. 788-795, 2008.

[2] M. J. van Osch, W. M. Teeuwisse, M. A. van Walderveen, J. Hendrikse, D. A. Kies and M. A. van Buchem, "Can Arterial Spin Labeling Detect White Matter Perfusion Signal?," *Magnetic Resonance in Medicine,* pp. 165-173, 2009.

[3] W.-C. Wu, S.-C. Lin, D. J. Wang, K.-L. Chen and Y.-D. Li, "Measurement of Cerebral White Matter Perfusion Using Pseudocontinuous Arterial Spin Labeling 3T Magnetic Resonance Imaging – an Experimental and Theoretical Investigation of Feasibility," *Public Library of Science One,* vol. 8, no. 12, 2013.

[4] R. Pohmann, "Accurate, Localized Quantification of White Matter Perfusion With Single-Voxel ASL," *Magnetic Resonance in Medicine,* vol. 64, no. 4, pp. 1109-1113, 2010.

[5] R. Pohmann, B. Künnecke, J. Fingerle and M. von Kienlin, "Fast Perfusion Measurements in Rat Skeletal Muscle at Rest and During Exercise with Single-Voxel FAIR (Flow-Sensitive Alternating Inversion Recovery)," *Magnetic Resonance in Medicine,* vol. 55, no. 1, pp. 108-115, 2006.

[6] J. R. Gawryluk, E. L. Mazerolle and R. C. N. D’Arcy, "Does functional MRI detect activation in white matter? A review of emerging evidence, issues, and future directions," *Frontiers in Neuroscience,* vol. 8, 2014.

[7] N. K. Logothetis, J. Pauls, M. Augath, T. Trinath and A. Oeltermann, "Neurophysiological investigation of the basis of the fMRI signal," *Nature*, vol. 412, no. 6843, pp. 150-157, 2001.

[8] T. T. Liu and G. G. Brown, "Measurement of cerebral perfusion with arterial spin labeling: Part 1. Methods," *Journal of the International Neuropsychological Society,* vol. 13, no. 3, pp. 517-525, 2007.

[9] Siemens Medical Solutions, "MR Basics - Magnets, Spins and Resonances," 2003. [Online]. Available: http://www.healthcare.siemens.com/magnetic-resonance-imaging/magnetom-world/publications/mr-basics. [Accessed 20 May 2014].

[10] R. Pohmann, "Physical Basics of NMR," in *In vivo NMR Imaging: Methods and Protocols*, Totowa, NJ, USA, Springer Science, 2011, pp. 3-21.

[11] P. Storey, "Introduction to Magnetic Resonance Imaging and Spectroscopy," in *Magnetic Resonance Imaging - Methods and Biological Applications*, Totowa, New Jersey, Human Press, 2006, pp. 3-59.

[12] D. Weishaupt, V. D. Köchli and B. Marincek, How Does MRI Work? An Introduction to the Physics and Function of Magnetic Resonance Imaging, Springer, 2006.

[13] R. B. Buxton, "The physics of functional magnetic resonance imaging (fMRI)," *Reports on Progress in Physics,* vol. 76, no. 9, 2013.

[14] G. G. Brown, J. E. Perthen, T. T. Liu and R. B. Buxton, "A Primer on Functional Magnetic Resonance Imaging," *Neuropsychology Review,* vol. 17, no. 2, pp. 107-125, 2007.

[15] "Basic NMR phenomena, MR data acquisition methods (pulse sequences), and key instrumentation," [Online]. Available: http://199.116.233.101/mitnecwiki/index.php/Basic_NMR_phenomena,_MR_data_acquisition_methods_%28pulse_sequences%29,_and_key_instrumentation. [Accessed 27 October 2014].

[16] J. P. Wansapura, S. K. Holland, R. S. Dunn and W. S. Ball, "NMR Relaxation Times in the Human Brain at 3.0 Tesla," *Journal of Magnetic Resonance and Imaging,* vol. 9, no. 4, pp. 531-538, 1999.

[17] Radiopaedia.org, "K space," [Online]. Available: http://radiopaedia.org/articles/k-space. [Accessed 23 October 2014].

[18] P. Tofts, Quantitative MRI of the Brain: Measuring Changes Caused by Disease, Wiley, 2004.

[19] D. W. McRobbie, E. A. Moore, M. J. Graves and M. R. Prince, MRI from Picture to Proton, Cambridge University Press, 2007.

[20] American Society of Functional Neuroradiology, "Magnetic Resonance Spectroscopy," [Online]. Available: http://www.asfnr.org/magnetic_resonance.html. [Accessed 23 October 2014].

[21] B. Soussi, "Basic principles of MR Spectroscopy in Neurosciences," in *MRI Principles of the Head, Skull Base and Spine: A Clinical Approach*, Springer, 2002, p. Chapter 3.

[22] P. M. Matthews and P. Jezzard, "Functional magnetic resonance imaging," *Journal for Neurology, Neurosurgery & Psychiatry,* vol. 75, pp. 6-12, 2004.

[23] I. Tracey, "Brief Introduction to FMRI - Physiology," 1998. [Online]. Available: http://fsl.fmrib.ox.ac.uk/fmri_intro/physiology.html. [Accessed 25 January 2015].

[24] K. Uludag, D. J. Dubowitz and R. B. Buxton, "Basic Principles of Functional MRI," in *Clinical Magnetic Resonance Imaging*, 2005, pp. 249-287.

[25] A. L. Vazquez and D. C. Noll, "Nonlinear Aspects of the BOLD Response in Functional MRI," *Neuroimage,* vol. 7, no. 2, pp. 108-118, 1998.

[26] Siemens Medical Solutions, "Inline BOLD Imaging," [Online]. Available: https://www.healthcare.siemens.com/magnetic-resonance-imaging/options-and-upgrades/clinical-applications/inline-bold-imaging. [Accessed 25 January 2015].

[27] J. H. Duyn, "The future of ultra-high field MRI and fMRI for study of the human brain," *Neuroimage,* vol. 62, no. 2, pp. 1241-1248, 2012.

[28] J. A. Detre, "Arterial Spin Labeled Perfusion MRI," *Clinical Neurology,* pp. 6-12, January 2008.

[29] M. Wintermark and e. al., "Comparative Overview of Brain Perfusion Imaging Techniques," *Stroke,* vol. 36, pp. 83-99, 2005.

[30] D. S. Williams, J. A. Detre, J. S. Leigh and A. P. Koretsky, "Magnetic resonance imaging of perfusion using spin inversion of arterial water," *Proceedings of the National Academy of Sciences - Biophysics,* vol. 89, no. 1, pp. 212-216, 1992.

[31] A. C. Silva, B. Stefanovic and F. F. Paiva, "Arterial Spin Labeling Measurements of Cerebral Blood Flow: A Review Emphasizing Pulsed versus Continuous Approaches," 2006.

[32] J. A. Detre and D. C. Alsop, "Perfusion magnetic resonance imaging with continuous arterial spin labeling: methods and clinical applications in the central nervous system," *European Journal of Radiology,* vol. 30, no. 2, pp. 115-124, 1999.

[33] M. Kelly, "ASL Methods and Potential for phMRI," [Online]. Available: http://www2.warwick.ac.uk/fac/sci/statistics/staff/academic-research/nichols/presentations/gsk-neurophysics/kelly_aslmethods.pdf. [Accessed 27 October 2014].

[34] D. C. Alsop and J. A. Detre, "Reduced Transit-Time Sensitivity in Noninvasive Magnetic Resonance Imaging of Human Cerebral Blood Flow," *Journal of Cerebral Blood Flow and Metabolism,* vol. 16, no. 6, pp. 1236-1249, 1996.

[35] A. C. Silva and S.-G. Kim, "Perfusion-Based Functional Magnetic Resonance Imaging," *Concepts in Magnetic Resonance,* vol. 16A, no. 1, pp. 16-27, 2003.

[36] S.-G. Kim and N. V. Tsekos, "Perfusion Imaging by a Flow-sensitive Alternating Inversion Recovery (Fair) Technique: Application to Functional Brain Imaging," *Magnetic Resonance in Medicine*, vol. 37, no. 3, pp. 425-435, 1997.

[37] Functional MRI Laboratory - University of Michigan, "Arterial Spin Labeling," [Online]. Available: http://fmri.research.umich.edu/research/main_topics/asl.php. [Accessed 27 October 2014].

[38] F. Calamante, D. L. Thomas, G. S. Pell, J. Wiersma and R. Turner, "Measuring Cerebral Blood Flow Using Magnetic Resonance Imaging Techniques," *Journal of Cerebral Blood Flow and Metabolism,* vol. 19, no. 7, pp. 701-735, 1999.

[39] W.-C. Wu, M. Fernandez-Seara, J. A. Detre and F. W. Wehrli, "A Theoretical and Experimental Investigation of the Tagging Efficiency of Pseudocontinuous Arterial Spin Labeling," *Magnetic Resonance in Medicine,* vol. 58, no. 5, pp. 1020-1027, 2007.

[40] W. Dai, D. Garcia, C. d. Bazelaire and D. C. Alsop, "Continuous Flow Driven Inversion for Arterial Spin Labeling Using Pulsed Radiofrequency and Gradient Fields," *Magnetic Resonance in Medicine*, vol. 60, no. 6, pp. 1488-1497, 2008.

[41] N. Santos, P. Figueiredo and J. Sanches, "Bayesian optimization of perfusion and transit time estimation in PASL-MRI," in *Conference IEEE Eng Med Biol Soc.*, 2010.

[42] R. B. Buxton, L. R. Frank, E. C. Wong, B. Siewert, S. Warach and R. R. Edelman, "A General Kinetic Model for Quantitative Perfusion Imaging with Arterial Spin Labeling," *Magnetic Resonance in Medicine,* vol. 40, no. 3, pp. 383-396, 1998.

[43] T. Q. Duong, D.-S. Kim, K. Ugurbil and S.-G. Kim, "Localized cerebral blood flow response at submillimeter columnar resolution," *Proceedings of the National Academy of Sciences,* vol. 98, no. 19, pp. 10904-10909, 2001.

[44] J. R. Gawryluk, R. C. N. D'Arcy, E. L. Mazerolle, K. D. Brewer and S. D. Beyea, "Functional mapping in the corpus callosum: A 4T fMRI study of white matter," *NeuroImage,* vol. 54, no. 1, pp. 10-15, 2011.

[45] "Grey matter," [Online]. Available: http://www.princeton.edu/~achaney/tmve/wiki100k/docs/Grey_matter.html. [Accessed 28 October 2014].

[46] C. Pereira, *Neurobiologia I - Organization of the Nervous System*, Universidade de Coimbra, 2012.

[47] Clinical Medical Associates, Inc., "Corpus Callosum," [Online]. Available: http://clinanat.com/mtd/563-corpus-callosum. [Accessed 30 October 2014].

[48] My-MS.org, "Brain Anatomy - Part 2," [Online]. Available: http://my-ms.org/anatomy_brain_part2.htm. [Accessed 30 January 2015].

[49] S. Hofer and J. Frahma, "Topography of the human corpus callosum revisited—Comprehensive fiber tractography using diffusion tensor magnetic resonance imaging," *NeuroImage,* vol. 32, no. 3, pp. 989-994, 2006.

[50] S. F. Witelson, "Hand and sex differences in the isthmus and genu of the human corpus callosum: A postmortem morphological study," *Brain,* vol. 112, pp. 799-835, 1989.

[51] M. Iacoboni and E. Zaidel, "Interhemispheric visuo-motor integration in humans: the role of the superior parietal cortex," *Neuropsychologia,* vol. 42, pp. 419-425, 2004.

[52] R. C. N. D'Arcy, A. Hamilton, M. Jarmasz, S. Sullivan and G. Stroink, "Exploratory Data Analysis Reveals Visuovisual Interhemispheric Transfer in Functional Magnetic Resonance Imaging," *Magnetic Resonance in Medicine,* vol. 55, no. 4, pp. 952-958, 2006.

[53] M. A. Fernández-Seara, J. Wang, Z. Wang, M. Korczykowski, M. Guenther, D. A. Feinberg and J. A. Detre, "Imaging Mesial Temporal Lobe Activation During Scene Encoding: Comparison of fMRI Using BOLD and Arterial Spin Labeling," *Human Brain Mapping,* vol. 28, no. 12, pp. 1391-1400, 2007.

[54] University College London, "Cogent 2000," Institute for Cognitive Neuroscience, [Online]. Available: http://www.vislab.ucl.ac.uk/cogent_2000.php. [Accessed 21 May 2014].

[55] D. H. Brainard, "The Psychophysics Toolbox," *Spatial Vision,* vol. 10, pp. 433-436, 1997.

[56] S. Aslan, F. Xu, W. L. Peiying, J. Uh, U. S. Yezhuvath, M. van Osch and H. Lu, "Estimation of labeling efficiency in pseudo-continuous arterial spin labeling," *Magnetic Resonance in Medicine,* vol. 63, no. 3, pp. 765-771, 2010.

[57] G. Shajan, M. Kozlov, J. Hoffman, R. Turner, K. Scheffler and R. Pohmann, "A 16-channel Dual-Row Transmit Array in Combination with a 31-Element Receive Array for Human Brain Imaging at 9.4T," *Magnetic Resonance in Medicine,* vol. 71, pp. 870-879, 2014.

[58] W. S. Tae, N. Yakunina, T. S. Kim, S. S. Kim and E.-C. Nam, "Activation of auditory white matter tracts as revealed by functional magnetic resonance imaging," *Neuroradiology,* vol. 56, no. 7, pp. 597-605, 2014.

[59] E. W. Weisstein, "Bonferroni Correction," MathWorld - A Wolfram Web Resource, [Online]. Available: http://mathworld.wolfram.com/BonferroniCorrection.html. [Accessed 30 January 2015].

[60] Y. Yang, W. Engelien, H. Pan, S. Xu, D. A. Silbersweig and E. Stern, "A CBF-Based Event-Related Brain Activation Paradigm: Characterization of Impulse-Response Function and Comparison to BOLD," *NeuroImage,* vol. 12, no. 3, pp. 287-297, 2000.

[61] A. R. Wade, "The Negative BOLD Signal Unmasked," *Neuron,* vol. 36, no. 6, pp. 993-995, 2002.

[62] N. Harel, S.-P. Lee, T. Nagaoka, D.-S. Kim and S.-G. Kim, "Origin of Negative Blood Oxygenation Level-Dependent fMRI Signals," *Journal of Cerebral Blood Flow & Metabolism,* vol. 22, no. 8, pp. 908-917, 2002.

[63] Y. Koush, M. A. Elliott and K. Mathiak, "Single Voxel Proton Spectroscopy for Neurofeedback at 7 Tesla," *Materials,* vol. 4, no. 9, pp. 1548-1563, 2011.

[64] S. Aslan, H. Huang, J. Uh, V. Mishra, G. Xiao, M. J. P. van Osch and H. Lu, "White matter cerebral blood flow is inversely correlated with structural and functional connectivity in the human brain," *Neuroimage,* vol. 56, no. 3, pp. 1145-1153, 2011.